JACS Au
AN OPEN ACCESS JOURNAL OF THE AMERICAN CHEMICAL SOCIETY

pubs.acs.org/jacsau
Article

Electrochemical Observation and pH Dependence of All Three Expected Redox Couples in an Extremophilic Bifurcating Electron Transfer Flavoprotein with Fused Subunits

Debarati Das, Wassim El Housseini, Monica Brachi, Shelley D. Minteer,* and Anne-Frances Miller*

Cite This: JACS Au 2025, 5, 1689−1706
Read Online

ACCESS | Metrics & More | Article Recommendations | Supporting Information

ABSTRACT: Bifurcating enzymes employ energy from a favorable electron transfer to drive unfavorable transfer of a second electron, thereby generating a more reactive product. They are therefore highly desirable in catalytic systems, for example, to drive challenging reactions such as nitrogen fixation. While most bifurcating enzymes contain air-sensitive metal centers, bifurcating electron transfer flavoproteins (bETFs) employ flavins. However, they have not been successfully deployed on electrodes. Herein, we demonstrate immobilization and expected thermodynamic reactivity of a bETF from a hyperthermophilic archaeon, *Sulfolobus acidocaldarius* (*Sa*ETF). *Sa*ETF differs from previously biochemically characterized bETFs in being a single protein, representing a concatenation of the two subunits of known ETFs. However, *Sa*ETF retains the chemical properties of heterodimeric bETFs, including possession of two FADs: one that undergoes sequential 1-electron (1e) reductions at high E° and forms an anionic semiquinone, and another that is amenable to lower-E° 2e reduction, including by NADH. We found homologous monomeric ETF genes in archaeal and bacterial genomes, accompanied by genes that also commonly flank heterodimeric ETFs, and *Sa*ETF's sequence conservation is 50% higher with bETFs than with canonical ETFs. Thus, *Sa*ETF is best described as a bETF. Our direct electrochemical trials capture reversible redox couples for all three thermodynamically expected redox events. We document electrochemical activity over a range of pH values and reveal a conformational change coupled to proton acquisition that affects the electrochemical activity of the higher-E° FAD. Thus, this well-behaved monomeric bETF opens the door to bioinspired bifurcating devices or bifurcation on a chip.

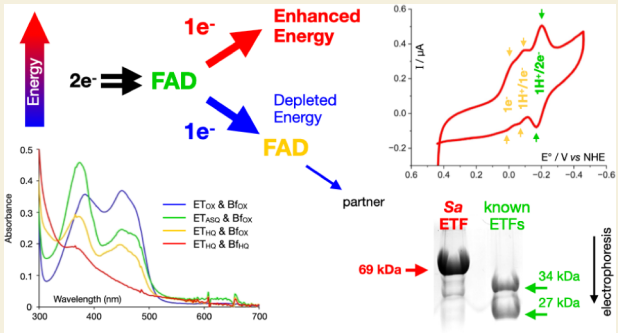

KEYWORDS: *hyperthermophilic, bifurcation, bifurcating electron transfer flavoprotein, direct electrochemistry, proton coupled electron transfer, spectroelectrochemistry, fusion enzyme*

1. INTRODUCTION

Electron transfer bifurcation ('bifurcation') concentrates energy from spontaneous reactions to yield energy-enriched products.[1−3] Thus, it is a highly desirable mechanism to incorporate into man-made devices. The fact that bifurcation is inherently an electron transfer reaction suggests that bifurcating enzymes could provide this functionality if they could be directly and efficiently coupled to electrodes.[4] Indeed, the advantages of enzymes have been exploited in bioelectrocatalytic devices to produce chiral amines based on abundant but inert N_2[5] and to capture CO_2 while also regenerating diffusible cosubstrates.[6]

Direct electrochemistry of bifurcating enzymes is a relatively new field. Catalytic current was observed from the inorganic clusters in bifurcating hydrogenase from *Thermotoga maritima*,[7] and square wave voltammetry (SWV) has been used to characterize the two [4Fe-4S] clusters of the bifurcating NADH-dependent ferredoxin:$NADP^+$ oxidoreductase from *Pyrococcus furiosus* (*Pf*Nfn).[8] However, only a single broad wave was observed for the three couples expected from the two flavins present. It was necessary to work with the large subunit alone, *Pf*NfnL, to resolve individual transitions from the bifurcating flavin.[9] Thus, bifurcating flavin sites have so far proven more difficult to study by direct electrochemistry.[10] Because bETFs contain only flavins, they are a good system in which to refine methods for bifurcating flavin sites. However, ETFs undergo an extensive conformational change as part of turnover,[11,12] so we tested the use of a conductive matrix to minimize constraints on protein movement while trapping the enzyme near the electrode surface and providing a large electroactive surface area with excellent electrical connectivity to the surface of glassy carbon electrodes.[13,14] Finally, because

Received: December 15, 2024
Revised: February 22, 2025
Accepted: March 17, 2025
Published: April 7, 2025

both the bifurcating systems in which direct electrochemistry has been successful were from hyperthermophiles,[7,9] we began with a hyperthermophilic bETF.

ETFs were first described in 1956 when a nonbifurcating ETF from the pig liver was characterized.[15,16] The initially described ETFs from mitochondria use a single flavin adenine dinucleotide (FAD) to convey single electrons from an acyl-CoA dehydrogenase to a quinone reductase, which in turn feeds respiratory electron transfer (canonical ETFs, cETFs). More recently, another group of ETFs has been recognized, containing two FADs. The one called the ET-FAD ('ET' for electron transfer) is analogous to the FAD of cETFs and gives one-electron (1e) equivalents to an acyl-CoA dehydrogenase or a quinone reductase at high reduction midpoint potentials (E°s). The additional FAD acquires a pair of reducing equivalents from NADH at lower E° and passes one to a lower E° (more reducing) acceptor in an endergonic reaction paid for by the exergonic transfer of the other electron to the ET-FAD (Scheme 1 and Figure 1). Thus, bifurcation confers

Scheme 1. Energy Landscape of Flavin-Based Electron Transfer Bifurcation in bETFs

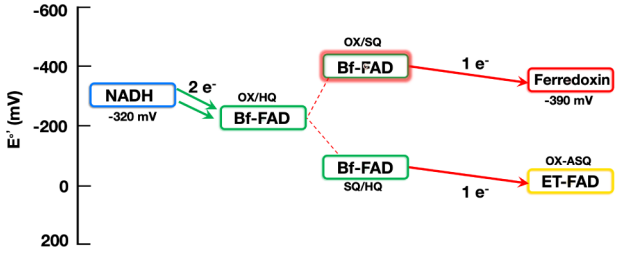

metabolic versatility by generating high-energy reductants required for demanding reactions such as CO_2 capture and N_2 fixation.[1,17−20] Crucially, it does so based on the abundant but less-potent reduced nicotinamide adenine dinucleotide (NADH). We want to harness bifurcation in electrocatalytic devices to exploit cheap, abundant fuel to drive demanding reactions.

Endergonic electron flow from NADH to ferredoxin is made possible by tight coupling to exergonic transfer from NADH to an acyl-CoA dehydrogenase or quinone oxidoreductase via the ET-FAD. The bifurcation event at the Bf-FAD (bifurcating FAD) must produce an electron more reducing than the receiving couple of the ET-FAD (electron transfer FAD), placing an upper limit of approximately −60 mV (note the orientation of the vertical axis in Scheme 1). Given the two-electron (2e) potential of Bf-FAD near −260 mV, this allows that the other one of Bf-FAD's virtual 1e couples can be as negative as −460 mV. This suffices to reduce many ferredoxins. Meanwhile, the Bf-FAD's E° is more positive than that of NADH, making its 2e reduction favorable, but with dissipation of only ≈ 60 mV. The high-energy ^{Bf}SQ (Bf-FAD semiquinone) generated upon transfer of 1e from Bf-FAD hydroquinone (^{Bf}HQ) to ET-FAD is not observed in intact systems except via transient methods,[21] consistent with being a transient high-energy state, but it enables the reduction of ferredoxin at the expense of NADH.

Thermodynamically, bifurcation requires that the two electron transfers be tightly coupled and that the exergonic transfer be sufficiently favorable to provide overall spontaneity. Efficient bifurcation also requires a mechanism that allows only 1e of each pair to access the exergonic path.[1,12,17,19,22] A flavin

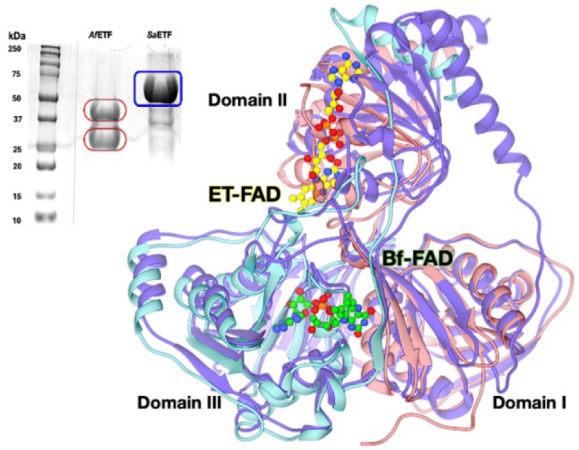

Figure 1. Structure of *Sa*ETF as predicted by AlphaFold.[34] A single polypeptide chain encompasses all the three domains of *Sa*ETF (purple) unlike the heterodimeric ETFs exemplified here by the ETF of *Acidaminococcus fermentans* (*Af*ETF) in which the EtfA subunit is in pink and EtfB is in teal (4KPU).[33] Domain I and domain III form the base on which mobile domain II rests. The AlphaFold model of *Sa*ETF predicts that three loops connect domain II to the base, in contrast to previously known heterodimeric ETFs where two loops connect them. The FADs are labeled with respect to their functions, as explained in the text. Inset: SDS PAGE gel image comparing the subunit composition of *Af*ETF, a heterodimer composed of subunits EtfA (larger) and EtfB (smaller), with the composition of *Sa*ETF which is composed of a single polypeptide corresponding to a fusion of EtfB followed by EtfA. A lane intervening between the *Af*ETF and the molecular weight standards was omitted for clarity; the image splice site is shown as a thin dashed line.

is a natural choice for the bifurcating site because the 1e reduced semiquinone (SQ) state of flavin is unstable, being populated to only 1% when free flavin is half-oxidized and half-reduced in aqueous solution.[10,23] Thus, the intrinsic reactivity of FAD is that of a two-electron (2e) carrier. Moreover, bifurcating ETFs (bETFs) appear to reinforce this via noncovalent interactions that further suppress the SQ states of the Bf-FAD that reacts with NADH (Figure 1).[24,25] However, the ET-FAD that carries 1e equivalents is subject to contrasting noncovalent redox tuning by the protein, stabilizing its anionic SQ (ASQ) state such that it accumulates to 90% of the population in the course of stepwise reduction.[24,26−30] The ET-FAD's unique reactivity enables it to restrict the exergonic path to only 1e, but the high $E°_{OX/ASQ}$ > $E°_{ASQ/HQ}$ constitutes very unusual reactivity for a flavin, and even the $E°_{ASQ/HQ}$ must be higher than usual to make the reaction favorable. Thus, ETFs in general, and bETFs in particular, are expected to have diagnostic FAD E°s, especially for the ET-FAD.[31−33]

ETFs are so far known to be heterodimeric flavoproteins, consisting of two subunits called EtfA and EtfB. Subunit A contributes domain I and most of domain II, whereas the smaller subunit B contributes domain III and two helices to domain II (Figure 1). Domains I and III are closely associated, forming the so-called 'base' of ETFs, whereas domain II is more loosely bound to the base and is believed to rotate by 80° in the course of turnover.[11,12] Domain II contains the ET-FAD, bound via equivalent noncovalent interactions in bETFs and cETFs. The Bf-flavin is situated in the interface between domains I and III, and the AMP portion of this FAD is bound

https://doi.org/10.1021/jacsau.4c01219
JACS Au 2025, 5, 1689−1706

in domain I in the same way as the structural AMP of cETFs, confirming the common ancestry of bETFs and cETFs.[33]

Spectroscopic, kinetic, and thermodynamic studies of bETFs support a mechanism in which NADH donates 2e in the form of a hydride to the lower-E° Bf-FAD, yielding its hydroquinone ^{Bf}HQ.[31,32,35−38] The ^{Bf}HQ transfers 1e exergonically to the ET-FAD, whereas the other 1e goes endergonically to ferredoxin or flavodoxin (Fd or Fld) at a lower E°. For these two transfers to be independent, an SQ state of Bf-FAD (^{Bf}SQ) would have to exist after the first transfer and before the second. However, such a species does not accumulate in intact bETF (it is 'suppressed'), indicating that it is high in energy and unstable. Proposed mechanisms nonetheless envision such an SQ as a transition state of sorts, as formally required upon transfer of 1e from ^{Bf}HQ to the ET-FAD. The virtual ^{Bf}SQ† is imagined to retain the energy difference between the exergonically transferred electron's starting and ending potentials, making it a more potent reductant than ^{Bf}HQ (Scheme 1). This in turn enables ^{Bf}SQ† to reduce lower-E° acceptors such as Fd.[33] Because the ^{Bf}SQ's reaction is more favorable than its formation, the two theoretical potentials are described as being crossed ($^{Bf}E^{o}_{OX/SQ}$ < $^{Bf}E^{o}_{SQ/HQ}$)(Scheme 1). Equivalently, for lack of a stable SQ state, Bf-FAD performs 2e chemistry. This is a critical signature of tight coupling between the two theoretical 1e ETs and is a requirement for bifurcation. The contrasting chemical reactivities of the two flavins are crucial to their abilities to play complementary roles and enable bETFs to carry out bifurcation. Therefore, these reactivities establish testable criteria for a flavoprotein to be considered a bETF. To establish the feasibility of incorporating bETF into devices, we tested for these signatures of reactivity upon entrapping *Sa*ETF on an electrode.

2. MATERIALS AND METHODS

2.1. Expression of *Sa*ETF

Monomeric *Sa*ETF was expressed based on a codon-optimized version of the gene AHC50813.1 from *Sulfolobus acidocaldarius* SUSAZ, equipped with an N-terminal His_6 tag and carried by a pET-based plasmid.[39] 10 mL of liquid culture of transformed Nico21 *Escherichia coli* was grown overnight at 37 °C and 250 rpm for 14−18 h in an incubator shaker (Innova 4330) and used to inoculate 1 L Terrific Broth supplemented with kanamycin (50 μg/mL). The 1 L culture was shaken at 180 rpm at 37 °C, and the OD_{600} was monitored periodically. Upon reaching an OD_{600} of 0.8, the temperature of the culture was lowered to 18 °C, and bETF gene expression was induced with 0.1 mM IPTG. The cells were grown overnight (14−18 h) at 180 rpm. Cells were then harvested by centrifugation (Thermo Scientific XTR Refrigerated Benchtop Centrifuge 75004521) at 4500 rpm, 4 °C, for 60 min, followed by a wash with pH 7.4 phosphate-buffered saline (137 mM NaCl, 2.7 mM KCl, 10 mM sodium phosphate monobasic, 1.8 mM potassium phosphate dibasic) before being frozen and stored at −20 °C.

2.2. Purification

Harvested cells (24−30 g from 1 L of culture) were thawed at 4 °C and resuspended in lysis buffer (2 mL/g pellet). The lysis buffer consisted of 20 mM sodium phosphate (pH 7.4), 300 mM NaCl, 1 mM (4-(2-aminoethyl)benzenesulfonyl fluoride)hydrochloride protease inhibitor (Chem Impex Intl #21250), 1 mM FAD (Chem Impex Intl #0051), and 1 μL each of lysozyme (Millipore 71110-1200KU) and DNase (Millipore 71205-25KUN). Cells were sonicated using a QSonic sonicator (Q125, 125W) at 50% amplitude in repeated cycles of a 10 s pulse followed by a 10 s pause, for 20 min. Lysed cells were centrifuged at 15000 g for 30 min in a refrigerated benchtop centrifuge (Thermo Scientific XTR 75004521). The supernatant was mixed with 2 mL of nickel nitrilotriacetic acid resin (Thermo Scientific 88222) pre-equilibrated with 5 column volumes (Cvols) of 20 mM sodium phosphate, 300 mM NaCl buffer (pH 7.4,'working buffer') augmented with 10 mM imidazole, with gentle stirring for 1 h at 4 °C. The slurry was then loaded into a column. The flowthrough was reloaded to ensure complete binding of the target protein to the resin. The resin was washed with 20 cv of working buffer augmented with 15 mM imidazole. The target protein was eluted with working buffer augmented with 150 mM imidazole. The eluted protein was concentrated to 3 mL using a centrifugal concentration cell (Amicon UFC801024, 30 kDa MWCO), and imidazole was removed by gel filtration on pre-equilibrated DG 10. The resultant protein was concentrated using a centrifugal filter and stored at −80 °C in aliquots of 50 μL.

2.3. Quantification of Protein and FAD

Protein was quantified using Pierce's A_{660} assay vs a standard curve of bovine serum albumin (BSA). FAD was quantified via the absorbance of flavin at 450 nm (A_{450}) and the corresponding extinction coefficient (ε_{450}) of 11300 $M^{-1}cm^{-1}$, after releasing the flavins from ETF.[38] To release the flavins, 400 μL of a 20 μM sample of ETF was denatured in the darkness at 100 °C for 10 min. The sample was cooled, and the denatured protein was spun down at high speed for 10 min.

2.4. Depletion of ET-FAD from *Sa*ETF

*Sa*ETF was found to have 2 FAD molecules per unit, as isolated. To deplete it of the more weakly bound ET-FAD, 100 μL of purified ETF was washed alternately with 400 μL of 1 M KBr in working buffer or working buffer alone, using a 0.5 mL centrifugal filter (10 kDa MWCO) spun at 14000 g for 15 min for each cycle in an Eppendorf 5417R Refrigerated Microcentrifuge. The alternating washes were repeated until the filtrate was no longer visibly yellow, indicating that no more ET-FAD was released.[40] Optical signatures of the filtrate and KBr-treated ETF were collected to confirm the complete removal of ET-FAD.

2.5. Reductive Titrations

Anaerobic reductive titrations were carried out in the inert N_2 atmosphere of a glovebox (Belle Technology, UK) at 4 °C. 400 μL of ETF samples at a final concentration of ≥ 10 μM were prepared. For NADH as a reductant, 2 equiv were required to completely reduce the ETF. The desired concentration of NADH required to completely reduce the ETF was prepared from stock solutions, whose concentration was measured by A_{340} and ε_{340} = 6220 $M^{-1}cm^{-1}$.[41] Titrations were carried out in self-masked cuvettes (Fireflysci, type 30BM, 700 μL, 5 mm path length) in a temperature-controlled sample holder (Quantum Northwest) monitored optically using an HP 8452A spectrophotometer refurbished and modernized by OLIS.

Reductive titrations with dithionite as a reductant were carried out in a similar fashion. Dithionite stock solutions (ε_{315} = 8.02 $mM^{-1}cm^{-1}$) were prepared in 0.02 M KOH solution (pH 11) inside the glovebox and diluted to the desired concentrations required to completely reduce the ETF.[42]

2.6. Determination of Midpoint Potentials via the Xanthine/Xanthine Oxidase Method

Reduction midpoint potentials were determined via spectroelectrochemistry using the xanthine/xanthine oxidase system to supply reducing equivalents slowly and continuously.[43,44] The reaction included catalytic amounts of methyl viologen as a mediator and a reference dye with a potential within ± 60 mV of the potential describing the event under study. The reference dye was required to undergo simultaneous reduction with the ETF, ensuring the two remained at equilibrium with one another throughout the reduction. Reference dyes were initially selected based on reported potentials, but extensive trials were necessary to identify dyes that coreduced with the ETF and equilibrated on the time scale of the reduction. The contents of each reaction were 400 μM xanthine, 20 μM ETF, 1 μM methyl viologen, and 1−5 μL of the reference dye, which was varied to obtain an optical signal that matched the amplitude of ETF's

https://doi.org/10.1021/jacsau.4c01219
JACS Au 2025, 5, 1689−1706

optical signal while minimizing obstruction to ETF's optical signal. Reactions were initiated by the addition of xanthine oxidase and monitored optically at 30 s intervals. The concentration of xanthine oxidase was varied from 10 to 100 nM, with larger concentrations used to achieve lower potentials.

Optical signatures were used to identify and quantify each state of the ETF during the reduction. For *Sa*ETF, the three E°s ${}^{ET}E^{\circ}_{OX/ASQ}$, ${}^{ET}E^{\circ}_{ASQ/HQ}$, and ${}^{Bf}E^{\circ}_{OX/HQ}$ were measured using methylene blue (E° = −33.25 mV), Nile blue (E° = −160.25 mV), and phenosafranin (E° = −296.25) at pH 8.5, respectively, calculated from published E°' values (E°' = 11 mV for methylene blue; E°' = −116 mV for Nile blue; E°' = −252 mV for phenosafranin, respectively)[30,44] (our notation uses a preceding superscript to identify the FAD to which the state descriptor or E° applies). The ETF solution was prepared at pH 7.4; however, after addition of the alkaline stock solution of xanthine, the pH was determined to be 8.5. Thus, the titration was conducted at pH 8.5, and the resulting E° values corresponding to pH 7.0 were calculated to permit comparison with literature values of E°' (see Discussion).[44] To obtain a lower pH, the concentration of NaOH used to dissolve xanthine was modified, within the limits imposed by xanthine's modest solubility.

Phase 1 was monitored on the basis of ET-FAD ASQ formation along with reduction of methylene blue, as indicated by absorbance gained at 374 nm and lost at 666 nm, respectively (Figure S1 provides flavin structures, S2 provides spectra). Maximal absorbance at 374 nm marked the completion of the reaction and was attained with decreased A_{454}, based on plots of A_{374} vs A_{454}. The absorbances at 666 nm for new methylene blue and 454 nm for the ETF were used to monitor the extent of reduction. The oxidized population (OX) and reduced population (= total − OX) were calculated for the ETF and the dye. Ratios of oxidized vs reduced populations for the ETF and dye were calculated at each step, $[FAD_{ox}]/[FAD_{ASQ}]$ and $[Dye_{ox}]/[Dye_{Red}]$, and analyzed using Nernst eq 1:

$$\ln \frac{[FAD_{OX}]}{[FAD_{RED}]} = \frac{n_{FAD}}{n_{Dye}} \ln \frac{[Dye_{OX}]}{[Dye_{RED}]} + n_{FAD} \frac{F(E^{\circ}_{Dye} - E^{\circ}_{FAD})}{RT} \quad (1)$$

where n_{FAD} and n_{Dye} are the stoichiometries of electrons acquired by the FAD and the dye upon reduction and *R*, T, and *F* are the ideal gas constant, the temperature in Kelvin, and Faraday's constant, respectively.

Plots of $\ln \frac{[FAD_{OX}]}{[FAD_{RED}]}$ vs $\ln \frac{[Dye_{OX}]}{[Dye_{RED}]}$ were used to determine the slope, which is equal to $\frac{n_{FAD}}{n_{Dye}}$ which in turn yields n_{FAD} since the $n_{Dye} = 2$. The determined n_{FAD} was then used with the known E°_{Dye} to solve for E°_{FAD} by equating the intercept to $n_{FAD}\frac{F(E^{\circ}_{Dye} - E^{\circ}_{FAD})}{RT}$ for the reaction under study.

The oxidized and reduced populations for phases 2 and 3 of *Sa*ETF were monitored at 454 nm for the flavin and 636 and 520 nm for Nile blue (phase 2) and phenosafranin (phase 3), respectively. The slopes for phases 1 and 2 are expected to be 0.5 for 1e flavin reduction, but a slope of 1 is expected for phase 3, for 2e reduction of flavins, since the dyes used undergo 2e reduction in all cases.

2.7. Direct Electrochemistry

Electrode preparation involved drop-casting *Sa*ETF onto the surface of a glassy carbon electrode (GCE, 0.07 cm^2) that had been precoated with multiwalled hydroxylated carbon nanotubes ($MWCNT_{OH}$). First, a solution of ethanol (1 mL) containing 1 mg of $MWCNT_{OH}$ (1 mg/mL) was sonicated for 5 h at 20 °C to ensure proper dispersion. Following sonication, 2 μL of the $MWCNT_{OH}$ solution was drop-cast onto the GCE, and the electrode was placed in an oven at 60 °C for 20 min to evaporate the ethanol completely and then cooled. One μL of a *Sa*ETF solution (6.25 mg/mL) was drop-cast onto the coated electrode surface. The electrode was then stored in a refrigerator at 2 °C for 1 h to allow complete adsorption of *Sa*ETF onto the $MWCNT_{OH}$ surfaces.

The *Sa*ETF solution used for drop-casting was prepared by diluting a stock solution of *Sa*ETF (62.5 mg/mL) that had been stored at −80 °C. The stock solution was diluted 10-fold using sodium phosphate buffer (pH 7). The diluted *Sa*ETF solution was stored at −20 °C until use.

Electrochemical tests were carried out using a three-electrode configuration, consisting of a platinum mesh as the counter electrode, a saturated calomel electrode (SCE) as the reference electrode, and the enzyme- and $MWCNT_{OH}$-modified GCE ('bioelectrode') as the working electrode. All experiments were performed in 50 mM sodium phosphate buffer prepared at the stated pH, with a total working volume of 10 mL. The solution was degassed with nitrogen for 25 min prior to each test. The desired temperature was obtained by placing the reaction vessel in a thermostated water bath pre-equilibrated at 20 or 40 °C, as indicated. Twenty min was allowed for the sample to stabilize at the set temperature. The bioelectrodes were evaluated by using cyclic voltammetry (CV) and square wave voltammetry (SWV) on a CH Instruments 650E potentiostat. CV measurements were generally conducted at a scan rate of 5 mV/s, while SWV was performed with an increment of 4 mV, an amplitude of 25 mV, and a frequency of 2.5 Hz (additional parameters were explored; see Figures S3−S9). Potentials were recalculated with respect to a normal hydrogen reference electrode (NHE) using the standard relation: $E_{NHE} = E_{SCE}$ + offset, where 0.244 V was used as the offset potential for all measurements at 20 °C, and 0.234 V was used as the offset potential for all measurements at 40 °C.

Phosphate buffers (50 mM) were prepared for trials at pH values of 6, 7, and 8, using ultrapure Milli-Q water (18 MΩ-cm). The required concentrations of the acidic and basic components, sodium dihydrogen phosphate (NaH_2PO_4) and disodium hydrogen phosphate (Na_2HPO_4), respectively, were calculated to achieve the target pH values. The solutions were prepared in volumetric flasks, with fine adjustments to pH made by the addition of small volumes of 1 M hydrochloric acid (HCl) or sodium hydroxide (NaOH). After pH adjustment, each solution was diluted to the final volume with Milli-Q water.

2.8. Diaphorase Assay

A 400 μL sample containing 15 μM *Sa*ETF and 30 μM *Af*Flavodoxin (*Af*Fld) was prepared in an inert atmosphere within a glovebox. The [NADH] concentration was increased in small steps of 1.5 μM each via 25 additions of a stock solution of 600 μM NADH, and an optical spectrum was collected after each addition to monitor the reduction of ETF and flavodoxin. To examine the effect of the concentration of reducing equivalents on the formation of *Af*Fld NSQ (^{Fld}NSQ), excess NADH was then added (up to 82.5 μM)

2.9. Informatics and Gene Neighborhood Analysis

The *Sa*ETF model shown in Figures 1 and 11 was generated using AlphaFold2 based on the amino acid sequence AHC50813.1 (GenBank).[34] The FADs were added based on individual domain-wise overlays with 4KPU,[33] and the result was refined by energy minimization using 100 steps of steepest descent followed by 10 steps of conjugate gradient minimization, as implemented in Chimera.[45−47]

Gene neighborhoods were produced and analyzed using the online tools provided by EFI-GNT.[48,49] This was done for a monomeric ETF and the EtfA subunit of heterodimeric ETFs. Since the vast majority of EtfA instances are immediately preceded by an EtfB, a separate analysis of EtfB occurrences was redundant. To generate a broad, unbiased dataset of *Sa*ETF homologues, the amino acid sequence AHC50813.1 (GenBank) was used as input for the retrieval of homologues from UniRef90 with a query e-value cutoff of 5 (UniProt: 2024-04/InterPro: 101). UniRef90 groups proteins differing by less than 10% from one another in a single node and uses the central sequence to represent the node. Fragments were excluded, and only bacterial and archaeal sequences were included because these genes have a greater tendency to be clustered with functional partners and a smaller tendency to be interrupted. This resulted in 904 unique sequences. Sequences 592−656 amino acid long were selected, and a network was constructed based on an alignment score threshold of 254, corresponding to a % identity of 70%. Lower values resulted in

https://doi.org/10.1021/jacsau.4c01219
JACS Au 2025, 5, 1689−1706

the clustering together of genes with different neighborhoods. The complete resulting sequence similarity network (SSN) grouped 105 nodes into 19 clusters, leaving 33 singletons, and is shown in Figure S10A. For each cluster, gene neighborhoods were constructed via screens including 10 genes on either side of the ETF gene. Diagrams showing the recurring features of the clusters are presented in the manuscript, and the nodes from which these derive are outlined in Figure S10B. Hub-and-spoke diagrams highlight neighbors identified for 80% or more of the sequences in a cluster, for clusters of 8 or more sequences, in Figure S10C.

For heterodimeric ETFs, amino acid sequences were retrieved based on the IPR001308 InterPro family for EtfA, sampled at a rate of 1/4 to yield 10915 unique sequences (no fragments). Sequences 300−338 amino acid long were selected from bacteria and archaea, and a network was constructed based on an alignment score threshold of 119, corresponding to a % identity of 70%. The complete resulting sequence similarity network (SSN) grouped 8275 nodes into 531 clusters, leaving 1291 singletons, and is shown in Figure S11A. To facilitate analysis while preserving the structure of the network, nodes sharing 75% identity or higher were united to reduce the network to 3441 nodes representing 8275 accession IDs. Gene neighborhood diagrams showing the recurring features of selected clusters are shown in the manuscript, and the nodes from which these derive are outlined in Figure S11B. For each cluster, gene neighborhoods were constructed by screening 10 genes on either side of the ETF gene. Diagrams were truncated for display, retaining and highlighting genes identified as recurring neighbors of monomeric ETFs (above). Hub-and-spoke diagrams highlight neighbors identified for 80% or more of the sequences in a cluster, for clusters of 8 or more sequences, in Figure S11C.

3. RESULTS

3.1. Composition of the ETF from *Sulfolobus acidocaldarius*

Overexpression of a codon-optimized version of the gene AHC50813.1 (GenBank, *Sulfolobus acidocaldarius* SUSAZ) in *E. coli* yielded *Sa*ETF as a soluble protein.[39] Sodium dodecyl sulfate polyacrylamide gel electrophoresis (SDS-PAGE) confirmed the presence of a single large polypeptide, as opposed to the two smaller subunits that make up previously characterized ETFs, exemplified in Figure 1 by the bETF of *Acidaminococcus fermentans* (*Af*ETF). The FAD:ETF stoichiometry was 2.0 (Table 1), identifying *Sa*ETF as a bETF rather than a cETF. FAD was not lost in the course of purification, in contrast to the case for other bETFs and other bifurcating enzymes characterized by direct electrochemistry.[7,9,33,38]

Table 1. Composition of *Sa*ETF Compared to That of *Af*ETF

	Yield (mg/L culture)	FAD/ETF Stoichiometry idea l = 2	Ratio band II/band I intensities
*Sa*ETF	48 ± 2	2.0 ± 0.03	0.986 ± 0.004
*Af*ETF	10 ± 1	2.0 ± 0.08	0.876 ± 0.007

The optical spectrum of *Sa*ETF has characteristic bands at λ_{max} = 454 nm (band I) and 384 nm (band II). *Sa*ETF's band I has a long-wavelength shoulder that is also seen in the FAD standard, so it is attributed to the unresolved vibrational structure known for free flavin.[50] A shoulder is also seen on the long-wavelength side of band II, which is not normally resolved for mesophilic bETFs such as *Af*ETF. This could also represent the offset between the band II of the two flavins, as the ET-FAD's band II occurs at a longer wavelength than that of the Bf-FAD, as in mesophilic ETFs.[30]

Observed spectra were deconvoluted into the contributions of each of the two flavins (Figure 2B). The Bf-FAD spectrum observed in ET-FAD-depleted *Sa*ETF shows band II with a λ_{max} value of 378 nm that is lower in amplitude than band I, whereas the λ_{max} of band II of ET-FAD is at λ_{max} = 394 nm, and the amplitude of band II is higher than that of band I (compared with the spectrum of the FAD standard). The differences between the two FADs do not stem from chemical modification, as flavins released from *Sa*ETF have almost the same spectrum as the authentic FAD standard (Figure 2B). Instead, the altered λ_{max}' and intensity ratios must reflect the polypeptide environments produced by the *Sa*ETF protein. Indeed, the shift of band II to shorter wavelengths for Bf-FAD is consistent with the smaller solvent exposure of this flavin,[50] whereas the red-shifted band II produces a shallower dip between bands I and II for ET-FAD. These distinctive spectral signatures resemble those seen in bETFs from *Rhodopseudomonas palustris* (*Rp*ETF), *Megasphaera elsdenii* (*Me*ETF), and *Af*ETF, indicating that the environments provided by *Sa*ETF are similar to those in other bETFs.[33,35,40,51] Moreover, the differences between the two flavins' signals have been reproduced computationally.[35] Some literature spectra of the ET-FAD lack the dip between bands I and II, but this can signify the accumulation of some 8-formyl flavin at that site.[52,53]

3.2. Chemical Reactivities of the Two FADs

bETFs are characterized by distinct complementary reactivities of their two flavins. In order to qualify as a bETF, the new monomeric ETF should have one high-E° FAD that undergoes two sequential 1e reductions, in which ASQ is the intermediate (ET-FAD). The other FAD should undergo a 2e reduction at a single lower E°.[31] Moreover, this second FAD is reducible by NADH (Bf-FAD).

Reduction by the 1e donor dithionite produced an initial increase in the intensity of band II at 374 nm accompanied by a drop in the intensity of band I at λ_{max} 454 nm. These changes are consistent with the conversion of oxidized (OX) flavin to ASQ, although a small population of the SQ may be produced in the neutral form (NSQ) based on a small increase in absorbance near 650 nm.[31] Attribution to a single event is confirmed by the clean isosbestic phase at 388 nm. This phase is charted in the inset as a line from large to lower ε_{450} (i.e., right to left) that also rises from mid to higher ε_{372}.

Further reduction caused simultaneous diminution of the intensities of band I and band II, with isosbestic points at 340 and 508 nm, consistent with the reduction of ASQ to HQ.[31] Indeed, the difference spectrum associated with this phase is dominated by a negatively signed spectrum of ASQ (Figure 3C), as is also seen in phase 2 of the reduction of other bETFs.[38] The last phase of reduction also involved a loss of absorbance in both bands I and II, but with different maximally affected wavelengths, more characteristic of the consumption of OX flavin and the formation of HQ (isosbestic points at 350 and 500 nm). Since this conversion occurred later, it is attributed to a flavin with a lower E°. Phase 3 is thus assigned to the reduction of Bf-FAD from OX to HQ. The natures of the three reductive phases seen for *Sa*ETF are documented by the corresponding difference spectra in Figure 3C. These resemble those seen in other bETFs, including those of *Pyrobaculum aerophilum* ETF (*Pa*ETF), *Rp*ETF, *Me*ETF, and *Af*ETF.[31,33,38,54] Thus, the two FADs of *Sa*ETF possess the thermodynamic reactivity required for bifurcating activity. Moreover, based on the shared spectral features, the

https://doi.org/10.1021/jacsau.4c01219
JACS Au 2025, 5, 1689−1706

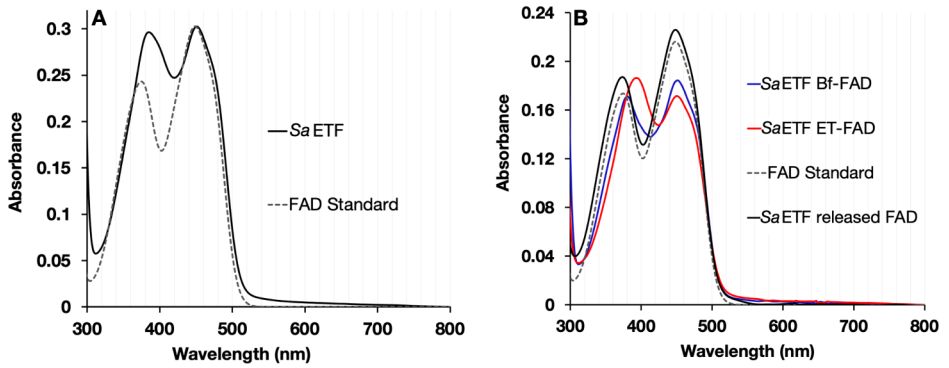

Figure 2. Visible spectrum of *Sa*ETF retains the spectral signatures of bETFs. (A) visible spectrum of 15 μM *Sa*ETF compared to that of a standard of purchased FAD. (B) Visible spectra of individual flavins in *Sa*ETF, flavin released from *Sa*ETF and the standard FAD, all normalized to 20 μM.

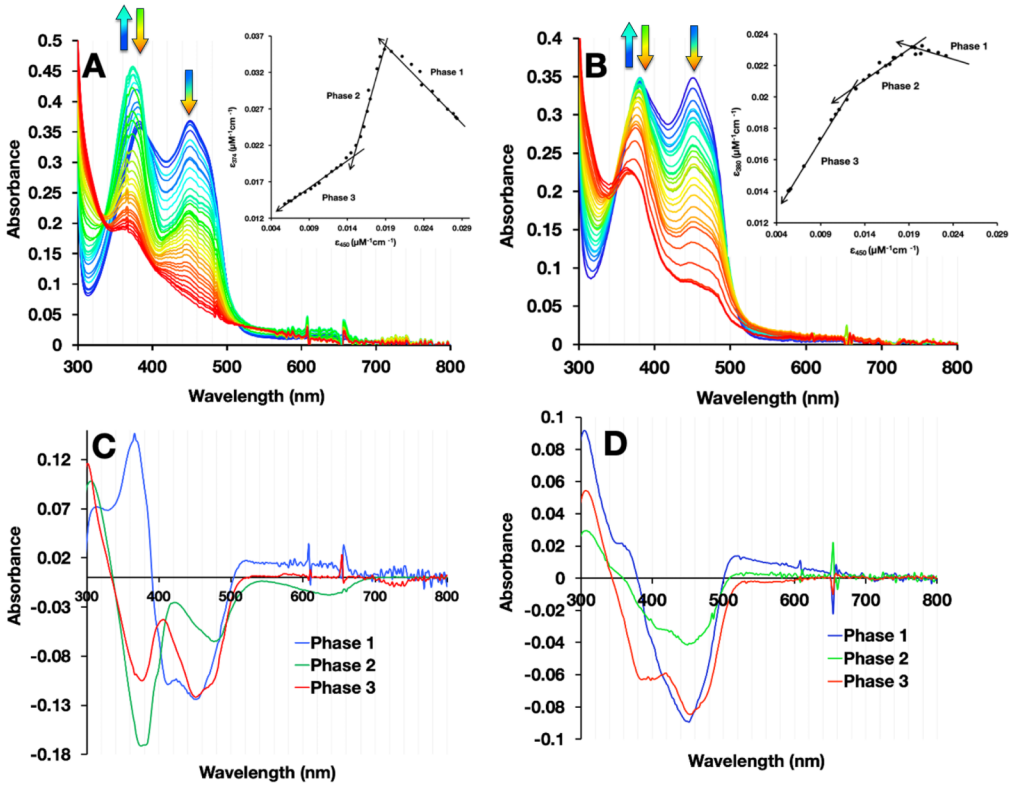

Figure 3. Contrasting reactivities of two flavins in *Sa*ETF upon stepwise reduction with (A) dithionite and (B) NADH and difference spectra of individual phases in reductive titrations of *Sa*ETF with (C) dithionite and (D) NADH. Initial reduction ET-FAD occurs in sequential 1e events, whereas subsequent reduction of Bf-FAD occurs in a single 2e reaction. 306 μM dithionite (A) or 500 μM NADH (B) was added in 1 μL aliquots to 400 μL of *Sa*ETF. Initial spectra are in blue, and final spectra (fully reduced *Sa*ETF) are in red as also indicated by the color gradients in arrows that indicate direction of amplitude change with increasing reduction. Reductive titration with dithionite as a reducing agent yields more ET-FAD ASQ, and phase 1 is better resolved from phase 2 in reduction with dithionite. Insets are plots of ε_{374} vs ε_{450} representing overall amplitude of band II where ASQ is strongest, vs overall amplitude of band I where OX is strongest. These thus visualize shifts of population from OX to ASQ and then to weakly absorbing HQ as the titration advances. The first point is at the right edge (largest ε_{450}), and the last point of the titration is at minimum ε_{450} on the left.

environments experienced by *Sa*ETF's two flavins resemble those present in other bETFs.

We also characterized stepwise reduction by NADH, which is the natural substrate for bETF. As seen in other bETFs, the maximum yield of ET-FAD ASQ (^{ET}ASQ) was lower with this 2e donor than with 1e donation,[29,36] although ASQ formation was confirmed by the fact that band II did not decrease in parallel with band I during initial reduction, and increased absorbance attributable to ASQ was seen in the uncongested longer-wavelength region from 500 to 550 nm (Figure 3B).[29,36] The lower population of ^{ET}ASQ is also evident in the difference spectra associated with phases 1 and 2 (Figure 3D) as well as the much gentler slope in the plot of ε_{380} vs ε_{450} (inset to Figure 3B). Nevertheless, the fact that the ET-flavin was reduced at all identifies *Sa*ETF as a bETF, because cETFs do not react with NADH.[35,38]

Since ETFs containing only ET-flavin do not react with NADH, Bf-FAD is the presumed site of reduction in this case. We confirmed this experimentally by adding NADH to *Sa*ETF that had been depleted of ET-FAD (Figure 4). During this

https://doi.org/10.1021/jacsau.4c01219
JACS Au 2025, 5, 1689−1706

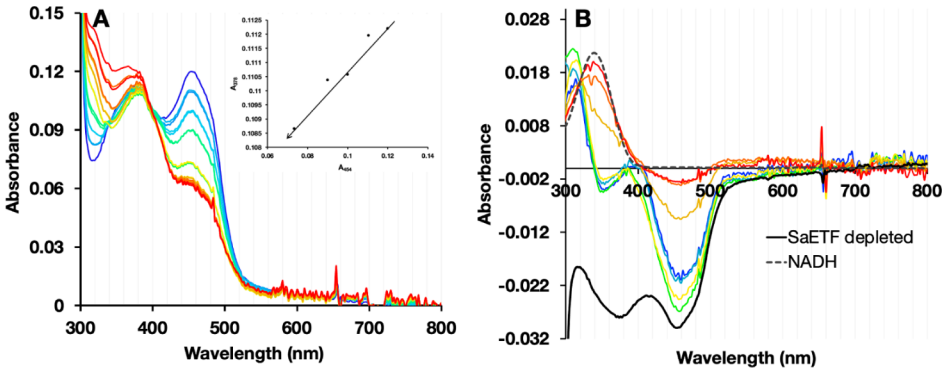

Figure 4. FAD that demonstrates $2e^-$ reactivity is confirmed to be Bf-FAD. 15.4 μM ET-FAD-depleted *Sa*ETF (15.4 μM) was reduced using 1 equiv of NADH. (A) Spectral changes during stepwise reduction of ET-FAD-depleted *Sa*ETF representing a single $2e^-$ reaction with a clear isosbestic at 400 nm. Inset plot of A_{378} vs A_{454} shows a dramatic drop at 454 nm compared to a modest drop at 378 nm (compare scales of axes). (B) Difference spectra resembling those of phase III (reduction of oxidized Bf-FAD, ^{Bf}OX, to Bf-FAD hydroquinone, ^{Bf}HQ).

stepwise reduction, there was no evidence of SQ formation, as confirmed by the absence of amplitude at wavelengths >520 nm and the plot of A_{380} vs A_{454} (inset to Figure 4A) demonstrating a simultaneous drop at both 454 and 378 nm. Difference spectra also resemble that of phase 3 in replete ETF, wherein the amplitudes of both bands I and II dropped, although the diminution of band II was less striking due to the absorbance of added NADH at 340 nm, especially after later additions.[31,38,54]

Interestingly, no charge-transfer (CT) band was observed between 600 and 800 nm, although such is commonly observed for flavin anionic hydroquinone and NAD^+ in other bETFs.[31,36,54] Nevertheless, these reductive titrations confirm that the Bf-FAD reacts with NADH and does not accumulate SQ. Thus, the two flavins of *Sa*ETF each display the reactivities expected of a bETF.

3.3. Quantitation of Reactivity: Reduction Midpoint Potentials of the FADs

Although the E°s of flavins in enzymes collectively span approximately 500 mV, the E°s of the flavins in bETFs fall within characteristic ranges, as required by the chemistry these enzymes mediate.[30,38,55] To determine E°s for each of the three events documented above, xanthine oxidase was used to provide a slow, continuous supply of reducing equivalents based on xanthine.[43,44] After screening numerous dyes, we adopted the use of methylene blue, Nile blue, and phenosafranin for phases 1, 2, and 3, respectively, because these dyes underwent reduction concurrent with the ETF, reflecting E°s close to ETF's for the phase in question.

For each phase, the ratio of the fraction of flavin oxidized divided by the fraction reduced was plotted vs the analogous ratio for the dye as $\ln(F_{ox}/F_{red})$ vs $\ln(D_{ox}/D_{red})$ in Figure 5. The best-fit lines display slopes close to 0.5 for each of phases 1 and 2, consistent with sequential 1e reductions of ET-FAD, since the dye used underwent 2e reduction. These results agree with the observed spectral signatures that best matched expectations for the OX → ASQ and ASQ → HQ transitions (above). Similarly, the slope of 1.0 in phase 3 in the presence of a 2e-accepting dye is consistent with 2e reduction of Bf-flavin and confirms the attribution made based on the difference spectrum associated with phase 3. The intercepts of the lines were used to calculate the E° of each phase using the Nernst equation (see Methods) and the known E° of the dye in use. The results are provided in Table 2 (see Discussion).

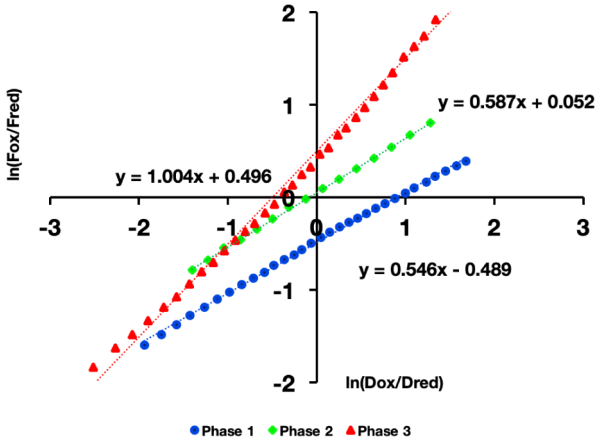

Figure 5. Plots of $\ln(D_{ox}/D_{red})$ vs $\ln(F_{ox}/F_{red})$ revealing 1e reactivity vs 2e reactivity from the slopes, and the midpoint potentials (E°s) from the intercepts via the Nernst equation. Uncertainties in slopes are on the order of 1% based on different titrations conducted on different *Sa*ETF preparations.

3.4. Direct Electrochemical Characterization of *Sa*ETF's Bf-FAD

The above spectroelectrochemical (spcEC) titrations were complemented by direct electrochemical characterizations (dirEC) that bypass the dependence on mediating dyes and explore the electrochemical properties of *Sa*ETF immobilized with hydroxyl-functionalized multiwalled carbon nanotubes ($MWCNT_{OH}$) on a glassy carbon electrode (GCE). Carbon nanotubes, particularly $MWCNT_{OH}$, significantly enhance the performance of enzyme-functionalized electrodes by improving electron transfer efficiency and stabilizing the protein.[56−58] We exploited this approach to make independent determinations of the E° values of *Sa*ETF and to characterize *Sa*ETF's direct electron transfer activity under different conditions, with a particular focus on the retention (or lack thereof) of the distinct reactivities of the two FAD cofactors. The redox activity of *Sa*ETF immobilized on $MWCNT_{OH}$-GCE (*Sa*ETF@$MWCNT_{OH}$) was assessed using cyclic voltammetry (CV, Figures 6, S3 and S5−S9) and square wave voltammetry (SWV, Figures 7 and S4).

https://doi.org/10.1021/jacsau.4c01219
JACS Au 2025, 5, 1689−1706

Table 2. E°s and pH Dependence Measured by Spectroelectrochemistry and Direct Electrochemistry[a]

	spcEC 4 °C			dirEC at 20 °C		dirEC at 40 °C
E° (mV)[a]	**Obs**, pH 8.5	**Obs**, pH 7.5 (20 °C)	**Calc**, pH 7.0	**Obs**, pH 8.5	**Obs**, pH 7.0	**Obs**, pH 7.0 (pH 6)
^{ET}OX-ASQ	−21.3 ± 0.2	−24 ± 1.0 (−21 ±2.9)	−21[b] ± 3			−61 ± 5 (−12)
^{ET}ASQ-AHQ	−161.4 ± 0.9	−104 ± 2	−74[c] ± 2			−127 ± 4 (−78)
^{Bf}OX-NHQ	−302.5 ± 4.6		−257[d] to −212.5[e]	−330 ± 5.2	−270 ± 7.4	−238 ± 6
$^{ET}K_{SQ}$	236	23				(13)
Max Pop SQ[f] (%)	88	71				(64)

[a]All potentials are vs NHE (normal hydrogen electrode). $E_{NHE} = E_{SCE} + 0.244$ V at 20 °C and $E_{SCE} + 0.234$ V at 40 °C. [b]Based on measurement at pH 7.5 and $0H^+/1e$, for $E°_{OX/ASQ}$ (0 mV/pH unit). [c]Based on measurement at pH 7.5 and $1H^+/1e$, for $E°_{OX/NSQ}$ and $E°_{ASQ/AHQ}$ (−60 mV/pH unit). [d]Based on measurement at pH 8.5 and $1H^+/2e$, for $E°_{OX/AHQ}$ (−30 mV/pH unit). [e]Based on measurement at pH 8.5 and $2H^+/2e$, for $E°_{OX/NHQ}$ (−60 mV/pH unit). [f]Using the definition of K_{SQ} and eq 3.

As an initial pH, we selected 8.5, consistent with the conditions used in the spcEC assays, and conducted the experiments at 20 °C using narrow low-E° scans to maintain the ET-FAD in its reduced state and focus on the Bf-FAD. CV measurements performed at a scan rate of 1 mV/s with $MWCNT_{OH}$ in the absence of *Sa*ETF showed no redox activity (Figure S3A). However, an identical $MWCNT_{OH}$-GCE electrode functionalized with *Sa*ETF displayed stable oxidation and reduction peaks at −330 ± 5.2 mV vs NHE at scan rates ranging from 0.5 to 100 mV/s (Figure 6A). These peaks were attributed to the Bf-FAD in *Sa*ETF based on agreement with the spcEC (−302.5 ± 4.6 mV) and correspond to nonturnover redox reactivity. As expected for an immobilized redox species, Figure S3C demonstrates a linear increase in peak current with increasing scan rate, from 0.5 to 100 mV/s.

The electron stoichiometry of a reaction can be determined from the CV peak width for immobilized species. At 20 °C, the ideal peak width at half-height for an immobilized redox couple is given by $89/n$, where n is the number of electrons transferred cooperatively.[59] For a fully cooperative two-electron transfer, where the SQ intermediate is highly unstable, the expected peak width is 45 mV for both oxidation and reduction.[60,61] As shown in Figure 6A, the observed peak widths range between 56 and 60 mV in both directions across all scan rates (Figure S3D). Furthermore, SWV experiments confirm these results, with obtained peak widths ranging between 62 and 70 mV (Figure S4). These values are significantly lower than 89 mV, strongly suggesting that the redox process involves the transfer of two electrons with considerable cooperativity. However, because the peak widths are greater than 45 mV, the two one-electron steps are not fully coupled to one another, so the sequential steps depicted in a Latimer scheme (eq 2) may

$$FAD_{OX} \xrightarrow{E°_{OX/SQ}} FAD_{SQ} \underset{E°_{OX/HQ}}{\xrightarrow{E°_{SQ/HQ}}} FAD_{HQ} \quad (2)$$

contribute mechanistically, even though we only observe the overall two-electron reduction potential $E°_{OX/HQ}$ which is the average of the two theoretical one-electron potentials, $E°_{OX/SQ}$ and $E°_{SQ/HQ}$.[10] These observations are consistent with the Bf-FAD accepting electrons pairwise from NADH but distributing them singly to two different acceptors in bifurcation.[61]

Figure 6B presents the nonturnover signals of *Sa*ETF's Bf-FAD recorded at pH values ranging from 6 to 8.5. In all cases, the peak widths remained within 56−60 mV in both directions, confirming the redox process as a two-electron transfer. Across this pH range, the calculated faradaic charge remains consistent, indicating that neither the attachment of *Sa*ETF nor the integrity of Bf-FAD is significantly altered (the background-subtracted charge under the current curve represents the total faradaic charge passed, with values of 1.443 ± 0.203 mC for the cathodic peak and 1.821 ± 0.324 mC for the anodic peak. This charge is directly proportional to the amount of electroactive *Sa*ETF adsorbed onto $MWCNT_{OH}$). Since the buffer was replaced between consecutive tests and the faradaic charges remained approximately constant, these results underscore the robustness of the *Sa*ETF immobilization strategy and its preservation of stable redox activity. However, based on SWV, the total faradaic charge attributable to Bf-FAD decreased with increasing pH (Figure S4B,C), suggesting that the shorter intervals of reduction (or oxidation) employed by SWV may be insufficient to fully (dis)charge all sites at high pH.

To determine how many protons are taken up upon the reduction of Bf-FAD in *Sa*ETF, Figure 6C plots Bf-FAD's $E°_{OX/HQ}$ ($^{Bf}E°_{OX/HQ}$) obtained by averaging the cathodic and anodic values from CVs recorded over the pH range of 6−8.5. $^{Bf}E°_{OX/HQ}$ decreases with increasing pH, with a slope of −56 mV per pH unit, as expected for a two-protons-per-two-electrons process ($2H^+/2e$). The proton stoichiometry indicates that Bf-FAD forms the neutral HQ state (NHQ), which is reasonable considering the pK_a for free flavin HQ is 6.7.[10] At pH 7.0, $^{Bf}E°'_{OX/HQ}$ = −270 mV, and across our pH range, $^{Bf}E°_{OX/HQ}$ remains consistently more positive than the $E°_{OX/HQ}$ of NADH. Thus, *Sa*ETF's Bf-FAD is thermodynamically predisposed to oxidize NADH, both by its capacity to accept two electrons in a coupled reaction and its $^{Bf}E°_{OX/HQ}$ that makes oxidation of NADH favorable, albeit with dissipation of only approximately 50 mV at pH 7. Because the NAD^+/NADH reaction is associated with only $1H^+/2e$, its E° drops by only −30 mV per pH unit, producing a slight increase in the driving force for NADH oxidation by ETF at lower pH. This may enhance catalytic efficiency and could be useful for optimizing bioelectrocatalysis in this system.

3.5. Direct Electrochemical Characterization of *Sa*ETF's ET-FAD

To characterize ET-FAD, we extended our potentials to more positive values to allow reoxidation of ET-FAD between scans. In the absence of *Sa*ETF, no redox activity was observed from the $MWCNT_{OH}$-GCE (Figure S5A). However, at room temperature and pH 6, immobilization of *Sa*ETF resulted in

https://doi.org/10.1021/jacsau.4c01219
JACS Au 2025, 5, 1689−1706

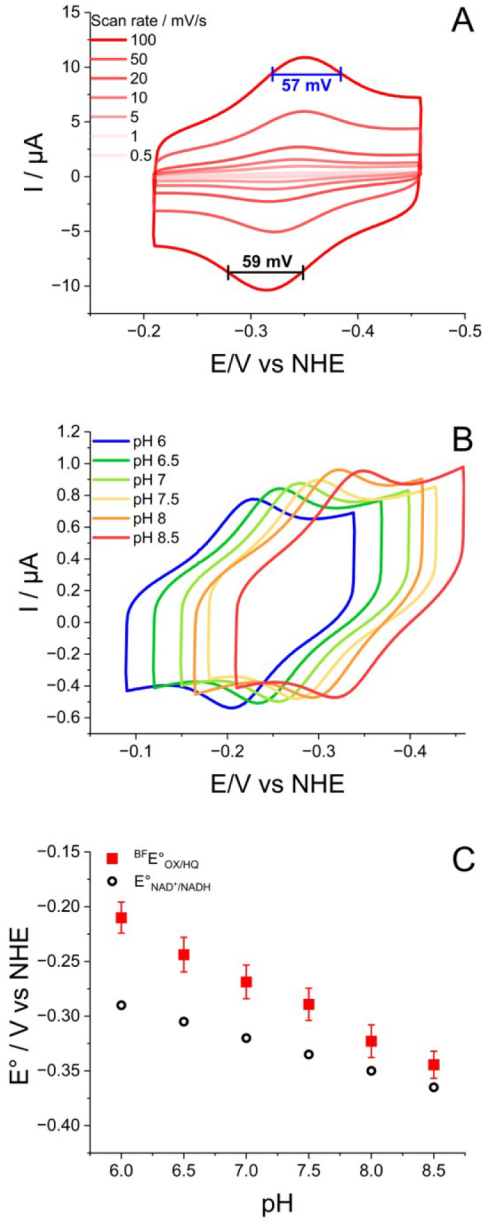

Figure 6. Direct electrochemistry of the Bf-FAD. (A) CV experiments performed at different scan rates (pH 8.5). (B) CV experiments conducted at different pHs (5 mV/s) and using the same electrode. (C) pH dependence of the E° of ^{Bf}OX/HQ, compared to the calculated pH dependence of the NAD^+/NADH redox couple, based on 1*H*/2e (−30 mV per pH unit) and E°' = −320 mV. Triplicate experiments were conducted at 20 °C, and the study of pH dependency was carried out using the same electrode.

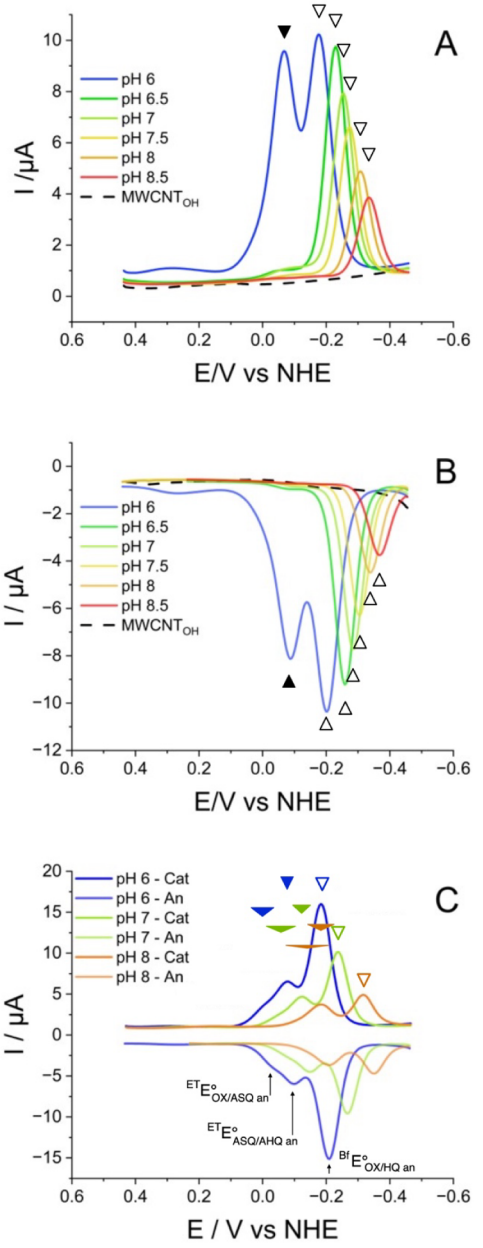

Figure 7. Square wave voltammetry (SWV) of both of the FADs, with signals attributed to Bf-FAD indicated by open triangles and signals attributed to ET-FAD indicated by solid triangles. This figure captures the behavior of both FADs because the CVs extended to much higher potentials than used in Figure 6. All experiments were carried out with an increment of 4 mV, an amplitude of 25 mV, and a frequency of 2.5 Hz. SCE was used as a reference electrode, and potentials have been recalculated with respect to NHE. (A) SWV at 20 °C showing cathodic traces and (B) SWV at 20 °C showing anodic traces. (C) SWV experiments performed at 40 °C to investigate the redox behavior of ET-FAD and Bf-FAD couples as a function of pH. A single electrode was used for all three pHs.

two distinct and reproducible peaks (SWV in Figure 7 and CVs in Figure S5). The midpoint potentials (E°) were measured as −77 ± 12 mV and −190 ± 15 mV at pH 6, as confirmed by CV (Figure S6A). The lower E° agrees with values for Bf-FAD obtained with different electrodes over different scan widths (Figure 6B). Therefore, the higher-E° peak is attributed to the ET-FAD, and because its integrated area and width are comparable to those of the ^{Bf}OX/HQ's peak at pH 6, the ET-FAD peak is similarly attributed to two electrons. Comparable SWV amplitude in both directions attests to reversibility (Figure 7A,B). No evidence of two sequential 1e steps was observed, even by CV at low scanning rates at 20 °C and pH 6, although separate events are observed at higher pH by spcEC (Figures 3 vs S5B).

To learn whether ET-FAD reduction is coupled to proton uptake, the investigation was extended to higher pH values (Figure 7A,B). SWVs at pH 6−8.5 revealed two striking phenomena. As in the narrower scans, Bf-FAD's SWV signal diminished in amplitude while shifting to more negative potentials at increasing pHs (Figure 7A, B), although CVs

https://doi.org/10.1021/jacsau.4c01219
JACS Au 2025, 5, 1689−1706

displayed pH-independent amplitude (Figure S6A). Second, the signal of ET-FAD disappeared altogether from SWV at pH values > 6.0, with only a small feature visible where ET-FAD's signal should have been at pH 6.5.

SWV suppresses capacitive contributions by driving a small potential change for only a short time (in our case, 25 mV in 0.2 s) before reversing the potential change. However, this amounts to 125 mV/s changes, so it may not detect conformations for which electron transfer is too slow, for example, due to an expanded distance between the nearest $MWCNT_{OH}$ and the flavin. However, CV employs a slower continuous scan, providing perspective on the cause of signal loss from SWV. The CVs in Figure S6A agree with SWV in that no signal is detected from ET-FAD at higher pH, despite the presence of a robust 2e signal at pH 6. However, at the intermediate pHs of 6.5 and 7, where the signal was already lost from SWV, CV showed a very broad feature. Despite its breadth, we attribute it to ET-FAD since it is lost at higher pHs in agreement with SWV for ET-FAD. Thus, the slower time-scale CV experiment suggests that ET-FAD transfers electrons increasingly slowly to/from the electrode at increasing pH, or that the population of the conformation that transfers electrons to the electrode is lower and/or accessed more slowly at high pH. Variation of the CV scan speed at pH 6 did not yield evidence of a rate-limiting conformational event (Figure S5B), and CVs performed in both the forward and reverse directions yielded identical results, confirming the reversibility and consistency of the shape of the broad electrochemical feature at pH 7 (Figure S7). Moreover, a CV scan at pH 6 collected after a scan at pH 8.5 demonstrated that the ET-FAD was not missing at pH 8.5, simply undetectable (Figure S6B). Thus, at higher pH, ETF may convert to a conformation that makes ET-FAD inaccessible to the conductive matrix. A pH-dependent conformational change seems plausible, since bETFs are known to alternate between a conformation in which the ET-FAD is exposed on the protein's surface and another one in which it is partially occluded in the interface between ETF's two domains (Figure 1).[12,62] Slow interconversion at 20 °C could allow CV to detect a broadened feature at intermediate pHs where the instantaneous population of accessible ET-FAD is too low to be significant via SWV. We hypothesize that as pH increases further, the frequency and extent to which ET-FAD makes tunneling contact with the conductive matrix drops to the point that it becomes undetectable even to CV.

A more gradual decrease in the Bf-FAD SWV signal vs increasing pH was also observed, but without any diminution or broadening of Bf-FAD's CV signal (Figures 7 vs S6A). Thus, all Bf-FAD retains contact with the conductive matrix on the time scale of CV. However, if ETF's association with the CNTs places the flavins at a longer tunneling distance at higher pH, slower electron transfer to the electrode could result in less charge transfer on the time scale of SWV. The large pH range over which the diminution in Bf-FAD SWV signal size occurs suggests a change in the interaction between the protein and the $MWCNT_{OH}$ as opposed to a protein conformational change, since the latter tends to be more cooperative and therefore abrupt. Further work with different varieties of MWCNTs and cosolvents that can modulate protein's adsorption onto the CNTs will explore the possibility of pH-dependent changes in the electrochemical efficiency of the adsorbed protein.

Despite the diminution in Bf-FAD's SWV signal size at high pH, its midpoint potential at pH 7.0 and 20 °C is estimated as $^{Bf}E^{\circ}_{OX/HQ} = -265 \pm 8$ mV, consistent with the findings above. At pH 6.0, the 2e E° attributed to ET-FAD at 20 °C is $^{ET}E^{\circ}_{OX/HQ} = -75 \pm 5$ mV.

Because the breadth of the ET-FAD CV signatures at pH 6.5 and 7.0 suggests conformational heterogeneity or rate-limiting conformational events, we repeated representative pH tests at a higher temperature of 40 °C. Figure 7C shows that at 40 °C, the ET-FAD peak can be described as two overlapping but distinct peaks at pH 6, suggesting that two separate 1e transfer events can indeed occur in adsorbed ETF, as in solution spcEC. Distinct shoulders could also be seen via CV at 40 °C and 5 mV/s (Figure S8), but slow scanning at 1 mV/s at pH 6 did not provide better resolution (Figure S9). At pH 7 and 40 °C, a shoulder can still be seen but is no longer resolved, and no shoulder is seen at pH 8 (Figure 7C). There is also a shift to lower E° with increasing pH, but given the decreasing size of the ET-FAD signal relative to the signal of the Bf-FAD, the ET-FAD may be dwindling in place as well as shifting. A conformational loss of electrochemical contact specific to the ET-FAD may thus be to blame, as at 20 °C. However, loss of the ET-FAD signal with increasing pH seems more gradual at 40 °C, possibly due to greater motional averaging at higher temperature.

The Bf-FAD's total SWV signal area also shrank significantly over the pH range, so our proposed pH-dependent association with the conductive matrix remains applicable at higher temperatures. We note that at 40 °C, SWV and CV both document the loss of electrochemical contact as pH rises for both FADs. This suggests that elevated temperature causes ETF to escape from electroactive adsorption more readily and to spend more time at distances greater than the tunneling length at higher pH in a process that appears thermally activated.

Because all features visible at 40 °C shifted to lower potentials with the elevation of pH, it appears that all three observed reductions are coupled to proton uptake. Therefore, the neutral ^{ET}SQ (^{ET}NSQ) is formed, consistent with the pH values of 6 and 7 at which this feature can be detected. It would then be consumed with the formation of ^{ET}NHQ. The 1e E° values suggested by SWV at pH 6 and 40 °C are −12 and −78 mV. For $^{Bf}E^{\circ}$, the $2H^+/2e$ stoichiometry obtained reproduces the stoichiometry observed at 20 °C. This most simply corresponds to the formation of NHQ from OX.

To the best of our knowledge, ours is the first observation of all three mechanistically expected redox events in an immobilized bifurcating enzyme. At pH 7 and 40 °C, the E° values obtained were $^{ET}E^{\circ}_{OX/SQ} = -61 \pm 5$ mV, $^{ET}E^{\circ}_{SQ/HQ} = -127 \pm 4$ mV, and $^{Bf}E^{\circ}_{OX/HQ} = -238 \pm 6$ mV. Detection of two resolved ET-FAD signals required the use of elevated temperature, but this need not be a kinetic effect. Moreover, because the change from 2e reactivity at 20 °C (Figure 7A blue curve) to at least some sequential 1e reactivity at 40 °C (Figure 7C blue curve) represents a change in the nature of the redox reactivity, it can have mechanistic significance. Specifically, it appears that the ^{ET}SQ state is more populated at higher temperatures at pH 6. Thus, the effect of temperature on the redox behavior of ET-FAD can be understood from a thermodynamic perspective. The separation of the single peak at pH 6 and 20 °C into two distinct peaks at 40 °C suggests a shift in the relative redox potentials ($E^{\circ}_{OX/ASQ} - E^{\circ}_{ASQ/AHQ}$) of the sequential one-electron transfers, in turn

https://doi.org/10.1021/jacsau.4c01219
JACS Au 2025, 5, 1689−1706

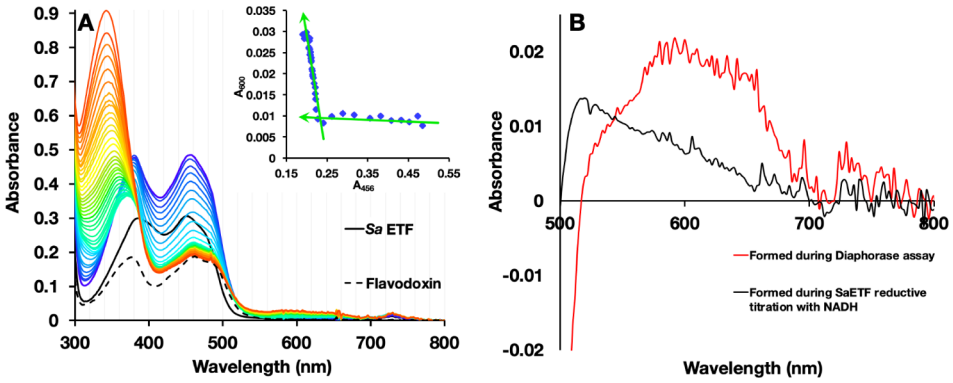

Figure 8. *Sa*ETF demonstrates diaphorase activity with respect to flavodoxin from *A. fermentans* (*Af*Fld). (A) Stepwise reduction of 30 μM flavodoxin and 15 μM *Sa*ETF with NADH. (B) Difference spectra comparing the NSQ species formed during the diaphorase assay (red) and the reductive titration of *Sa*ETF with NADH (black). Spectra represent the one collected at 120 μM NADH minus the starting spectrum for the difference spectrum reflecting diaphorase activity, whereas the black difference spectrum was obtained by subtracting the ox spectrum from the end of phase 1 spectrum during the reductive titration with NADH because this is the one with the maximum SQ content (as seen in Figure 3B).

indicating that $E^{\circ}_{OX/ASQ}$ and $E^{\circ}_{ASQ/AHQ}$ respond differently to temperature variation. Because the SQ formation constant $K_{SQ} = [SQ]^2/[OX][HQ]$ depends on $E^{\circ}_{OX/ASQ} - E^{\circ}_{ASQ/AHQ}$ (eq 3), such temperature dependence can explain the altered relative stability of the SQ. Higher temperatures can affect enzyme flexibility, the protonation states of nearby residues, and the hydration environment of the active site, all of which contribute to modulating redox potential differences.[63] Changes in entropic contributions at elevated temperatures may also affect the degree of electronic coupling between the flavin redox states, shifting the electron transfer pathway.

$$\Delta E^{\circ} = E^{\circ}_{OX/ASQ} - E^{\circ}_{ASQ/AHQ} = \frac{2.303RT}{F} log_{10}(K_{SQ}) \quad (3)$$

Thus, rather than attributing improved peak resolution solely to increased electron transfer rates, our results suggest that temperature may modulate the fundamental thermodynamics of the system, altering redox potential spacing and influencing the nature of the electron transfer process. Further investigations into enzyme conformational dynamics and protonation equilibria at varying temperatures should provide deeper insights into these effects. The complex pH dependence of *Sa*ETF electrochemistry reveals an interplay between protonation state, redox reactivity, and possibly enzyme conformational effects, which collectively regulate the redox properties of ET-FAD in particular.

3.6. *Sa*ETF Demonstrates Diaphorase Activity, albeit Low

To qualify as a bETF, *Sa*ETF's Bf-FAD should reduce two separate 1e acceptors based on the 2e donor NADH. The two reductions should be coupled, and the reduction of a high-E° acceptor should drive the reduction of a low-E° acceptor. The identity of *Sa*ETF's low-E° partner is not yet known, so a physiologically appropriate bifurcation assay is premature. However, we investigated the first of these criteria with a diaphorase assay of *Sa*ETF's ability to reduce Fld from *A. fermentans* based on NADH.[64] To do so, a mixture of 15 μM *Sa*ETF and 30 μM Fld was subjected to a stepwise reduction with NADH (1.5 μM increase per addition). In contrast to the case of ETF alone (Figure 3B) or Fld alone (Figure S12), a small but reproducible amount of NSQ formed, which was therefore attributed to the reduction of Fld by *Sa*ETF (Figure 8).

To test for diaphorase activity, successive additions of NADH produced increases in [NADH] by 1.5 μM each. As [NADH] increased to 9 μM, a slight shift of λ_{max} of band II from 382 to 380 nm was followed by a decrease in the height of band I at 456 nm. Although the absorbance of Fld's FMN, in addition to that of the Bf-FAD, obscured changes in ET-FAD's spectrum A_{450} dropped, while band II underwent negligible loss of amplitude at 380 nm, and the clear isosbestic point at 390 nm confirms the conversion of some ^{ET}OX to ^{ET}ASQ. Following considerable reduction of OX flavins, further additions of NADH to >10.5 μM caused the absorbance at both 380 nm (band I) and 456 nm (band II) to decrease, while a broad signal formed at 600 nm, mainly after full reduction of the ETF (Figure 8B). Although such a species could result from a Bf-FAD if its redox tuning is altered in a complex with the added Fld, our work has so far found that any association with Fld is transient, literature finds that the Bf-FAD E° is not affected, and that binding of Fd in fact suppresses SQ accumulation for the ET-FAD (as seen in Figure 8A).[32] Moreover, most flavin sites that stabilize SQ do so at E°s higher than that of Fld. The appearance of this NSQ at the most reducing points in the titration is therefore most consistent with the formation of Fld's OX NSQ based on electrons from *Sa*ETF.

The amount of ^{Fld}NSQ formed was less than stoichiometric relative to the NADH added, likely because *Af*Fld is not the natural partner protein of *Sa*ETF, so *Af*Fld may not be an efficient acceptor from *Sa*ETF.[65] In the absence of *Sa*ETF, Fld did not react with excess NADH (Figure S12). Nevertheless, Figure 8B shows that the NSQ that accumulates when *Sa*ETF is present with Fld is distinct from what is observed upon the reduction of *Sa*ETF alone. Thus, the formed NSQ is assigned to Fld, indicating that *Sa*ETF transfers 1e to Fld based on 2e accepted from NADH, similar to electron transfer in bifurcation.

3.7. Sequence Similarity Networks and Gene Neighborhood Analyses

To determine the physiological function of *Sa*ETF, we analyzed the genes that flank it.[66,67] For bETFs of known function, the ETF genes are flanked by those of their partner proteins: acyl-CoA dehydrogenases (ACADs), ETF/quinone oxidoreductase (ETF/Qor), or the homologous heterodimeric complex of FixC and FixX (FixCX), as seen for EtfA in Figure

https://doi.org/10.1021/jacsau.4c01219
JACS Au 2025, 5, 1689−1706

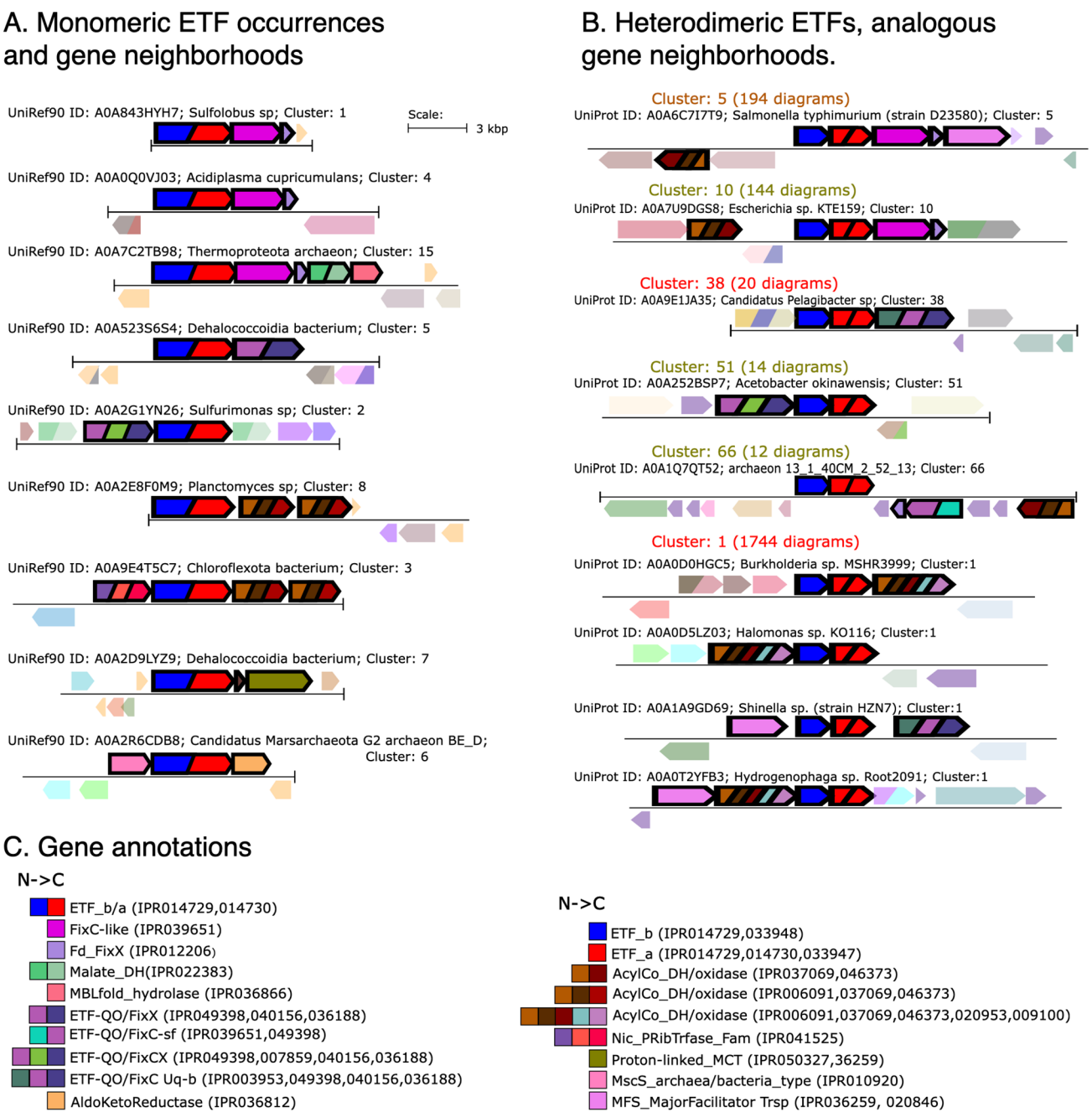

Figure 9. Gene neighborhoods of the *Sa*ETF gene. Panel A depicts the genes flanking *Sa*ETF homologues in major clusters of the SSN. When two clusters had very similar neighborhoods, only the more strongly populated cluster's typical neighborhood is shown. The diagrams are ordered according to the recurring neighbors. Thus, diagrams at the top show the ETF flanked on one or other side by genes for either ETF/Qor or its two-part homologue FixCX.[65,68] Diagrams below show the neighborhoods that feature ACADs and the two diagrams at the bottom show associations with a transmembrane channel or transporter. Panel B shows the occurrences of similar neighborhoods in bacteria where a conventional heterodimeric ETF has an established function. Again, ETF genes associated with a gene(s) for ETF/Qor or FixCX are shown near the top with clusters containing ACADs below. Panel C provides the color codes used for gene annotations in panels A and B. The related sequence similarity networks are in Figures S10 and S11.

9B. We therefore compared the gene neighborhoods of *Sa*ETF homologues with the neighborhoods of heterodimeric ETFs. Figure 9A shows the neighborhoods that typify different clusters of monomeric ETFs. Based on the widespread presence of genes for an ACAD, an ETF/Qor, and/or a FixCX pair nearby, the monomeric putative ETFs in the top seven diagrams can indeed be considered ETFs (Figure 9A). The lower two diagrams include other genes also seen near EtfA genes, such as transporters, but these less common contexts raise the possibility of new functions that are beyond the scope of the current investigation. Interestingly, Fld or Fd genes were not frequently found in the neighborhoods. Thus, these low-E° partners specific to bETFs appear not to colocate with EtfA and EtfB in most genomes. Overall, the colocation of monomeric ETF with ACADs, FixCX, or ETF/Qor indicates that it functions as an ETF.

Since cETFs also function with ACADs or ETF/Qors, and the low-E° partner exclusive to bETFs was not found as a

https://doi.org/10.1021/jacsau.4c01219
JACS Au 2025, 5, 1689−1706

neighbor, we employed amino acid sequence signatures to interrogate the bifurcating/nonbifurcating nature of *Sa*ETF. We used the consensus sequence of 310 bETFs or the consensus sequence of 449 cETFs[69] and performed pairwise alignments of each with *Sa*ETF. *Sa*ETF was 53% identical (69% similar) to the bEtfB consensus over *Sa*ETF's N-terminal residues 4−266, whereas its identity with cEtfB's consensus sequence was 29% (49% similarity) for residues 4−236 of *Sa*ETF (see below). In its C-terminal residues 287−607, *Sa*ETF was 49% identical (64% similar) to bEtfA's consensus sequence but only 33% identical (44% similar) to cEtfA's, over residues 344−600. Signature sequences proposed to differentiate bETFs from cETFs were also present in *Sa*ETF (not shown).[12,69] Thus, *Sa*ETF is best described as a bETF.

4. DISCUSSION

4.1. *Sa*ETF Concurs with bEtfs with Respect to FAD Content, Spectra, and Reactivity

*Sa*ETF is, to our knowledge, the first ETF for which all expected couples could be resolved by direct electrochemistry, and as such, it brings the possibility of incorporating bifurcating activity into bioelectrocatalytic devices. Our biochemical, spectroscopic, and electrochemical characterizations concur that *Sa*ETF is a bifurcating ETF. 1- *Sa*ETF incorporates two noncovalently bound FADs per molecule, the characteristic complement of bETFs. 2- The FADs display UV/visible spectral features characteristic of bETF FADs including the strong, red-shifted band II of the ET-FAD and the unresolved vibrational structure of the Bf-FAD's band I. These indicate flavin binding sites similar to those of known bETFs, consistent with sequence conservation. 3- The two FADs of *Sa*ETF furthermore display electrochemical activity characteristic of bETFs, consistent with the thermodynamic requirements for bifurcating activity. 4- We show that 2e reactivity with NADH resides in the Bf-FAD by treatment that removes the ET-FAD,[18,31,36] and our reductive titrations confirm that the Bf-FAD has a low 2e E° that is nonetheless higher than that of NADH and similar to the $^{Bf}E°_{OX/HQ}$ in other bETFs (red bar, Figure 10). Direct electrochemistry reveals complex conformational behavior responsive to pH and

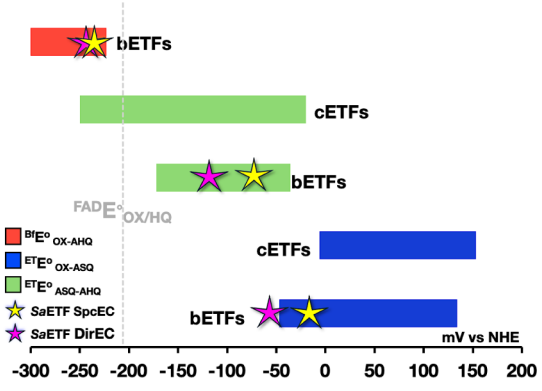

Figure 10. Comparison of E°s of the bETFs and cETFs. *Sa*ETF E° values for the three redox reactions are compatible with the E°s exhibited by nonmutated and flavin-replete bETFs, demonstrating bETF-like reactivity. *Sa*ETF spcEC values were measured at pH 8.5 and 4 °C and adjusted to pH 7 as in Table 2; dirEC values were measured at pH 7.0 at 40 °C. Literature E°' values are drawn from Sato et al.[38] and Supporting Information of Mohamed Raseek et al.[35]

temperature but supports spectroelectrochemistry's documentation of the two sequential high-E° couples of ET-FAD and the strong population of ASQ by this flavin, which are rare among flavoproteins generally but characteristic of ETFs. These findings and the gene neighborhood of *Sa*ETF justify the ETF name and attribution of bifurcating activity, but the protein deviates from all previously characterized ETFs in that it is monomeric rather than heterodimeric.

Redox enzymology abounds with examples of enzymes that contain different combinations of recurring functional modules.[70−73] Indeed, numerous EtfAs possess a ferredoxin-like domain fused to the N-terminus, as in *Aw*ETF.[11] The C-terminal domain of EtfA (domain II) is also one of the three domains of a butyryl-CoA reductase.[74] In bacterial and archaeal genomes, the vast majority of EtfA genes occur immediately following an EtfB gene, and similarly, the majority of EtfB genes precede a gene annotated as that of an EtfA (Figures 9 and S11). Thus, our identification of a monomeric version in which the two subunits are fused is a gratifying and expected discovery.

Bifurcation requires a higher-E° FAD that conducts two sequential 1e events. This is confirmed in *Sa*ETF and is notable because the ET-FAD is the one with the most perturbed E° values relative to the single 2e E° of free flavin at −207 mV.[10] This is, therefore, the flavin whose binding site must exert the strongest tuning. Thus, our finding that *Sa*ETF's $^{ET}E°_{OX/ASQ}$ and $^{ET}E_{ASQ/AHQ}$ determined by spcEC at pH 7.5 are in the ranges observed for other ETFs is most unlikely to be the result of chance (Figure 11). Indeed, the difference spectra associated with these events in *Sa*ETF resemble those established for the same events in other bETFs (Figure 3).[30]

Finally, although a biochemical assay of bifurcation must await the identification and purification of the physiological partners, we show that *Sa*ETF is able to distribute reducing equivalents acquired in pairs to different partners. The gene neighborhoods of *Sa*ETF homologues are replete with genes for high-E° partners documented in other bETF systems, but the identity of the low-E° partner is yet to be determined. Nevertheless, the amino acid sequence of *Sa*ETF has 50% higher homology with bETFs than with cETFs (Figure 11). Thus, all evidence in hand concurs that *Sa*ETF is a bETF.

4.2. *Sa*ETF FADs' Redox Reactivities Can Be Explained Based on Conserved Amino Acids

To learn whether *Sa*ETF shares the same function as bETFs (group II[69]), we investigated the anticipated corollary: that *Sa*ETF should share amino acid conservation with group II ETFs, especially near the flavins.[69] We used an AlphaFold model for *Sa*ETF,[34] color-coded according to amino acid conservation among a set of 48 bETFs distributed throughout group II and 24 monomeric ETFs related to *Sa*ETF (clusters 1, 4, 15, see Figure S10). As expected, based on the robust sequence conservation, AlphaFold generated the familiar ETF fold based on *Sa*ETF's sequence. The model aligns well with the crystal structure of *Af*ETF on a domain-by-domain basis, with RMSDs of 0.83, 0.83, and 0.86 Å, respectively, for 189 pruned atom pairs of the total 205 in domain I, 107 pruned pairs of the total 118 in domain II, and 169 pruned pairs of the 193 in domain III (see Figure 1B). Consistent with *Sa*ETF's conservation of typical bETF E° values, Figure 10A shows that amino acid conservation is high surrounding the FADs.

Both FADs play essential roles in bifurcation, but their different reactivities require different tuning, as evidenced by

https://doi.org/10.1021/jacsau.4c01219
JACS Au 2025, 5, 1689−1706

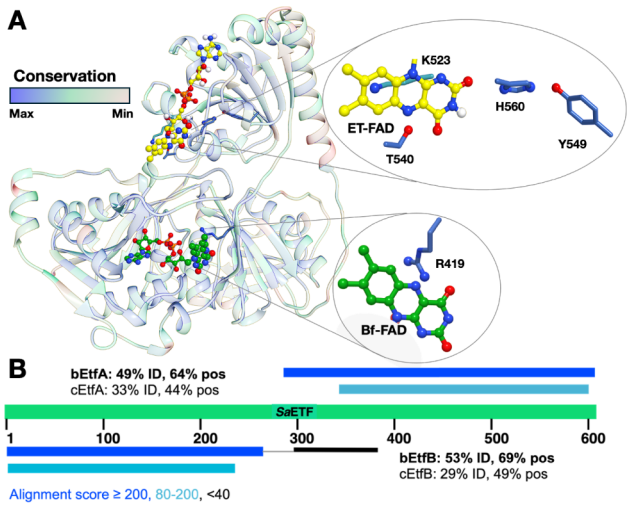

Figure 11. Degree of and distribution of amino acid conservation between *Sa*ETF and group II (bifurcating) ETFs. A An energy minimized AlphaFold model of *Sa*ETF with residues color-coded according to degree of conservation among a set of 24 SaETF homologues' and 48 nonbasal bETF sequences from group II.[69] Insets provide details of each of the two flavin sites, featuring residues documented to contribute to redox tuning for the ET- (yellow) and Bf-flavins (green). B Comparison of *Sa*ETF's amino acid sequence homology with bifurcating ETFs (bETFs) vs canonical ETFs (cETFs). Consensus sequences for each of bEtfA and bEtfB, and cEtfA and cEtfB were obtained from collections of group II and group I ETFs from which basal branches had been removed.[69] Pairwise BLAST-P alignments of *Sa*ETF with each of these yielded the results shown.

the contrast in amino acid conservation in their two sites (Figure 11A). Suppression of 1e reactivity is important for the Bf-FAD to minimize futile electron transfer to higher E°, which, in turn, requires suppression of SQ states.[1,17,37] Additionally, depression of $^{Bf}E°_{OX/HQ}$ maximizes the energy conserved from NADH. In the Bf site, the side chain of R419 of *Sa*ETF ($R419_{Sa}$) is close to the flavin N5, suggesting retention of a conserved H-bond to N5 seen in *Af*ETF via $R146_{Af}$. This interaction has been proposed to modulate Bf-FAD's reactivity in *Af*ETF[25] and has been shown to contribute to FAD binding in *Rp*ETF.[30] Thus, the disruption of this interaction abrogates bifurcation activity.

Efficient bifurcation also requires the passage of a single electron to the exergonic path for each pair of electrons acquired. Therefore, the ET-flavin must be a 1e carrier with a stable SQ. However, free flavin populates SQ at only 1% maximum and mostly as NSQ.[10] Thus, residues that stabilize the ASQ of ET-flavin play a critical role in producing ETF's essential activity,[30] and the resemblance of *Sa*ETF's spectral features and E° values to those of known bETFs predicts that the ET site should possess interactions similar to those elucidated in other ETFs.[24,75,76]

As anticipated, *Sa*ETF's modeled ET side retains residues held responsible for the unusually stable ASQ (Figure 11, inset).[24,29,33] $R273_{Af}$ is replaced by $K523_{Sa}$, $S290_{Af}$ by $T540_{Sa}$, $H290_{Af}$ by $H560_{Sa}$, and $Y279_{Af}$ by $Y549_{Sa}$. Electrostatic stabilization by R/K is understood to stabilize the ASQ and AHQ states. In the crystal structure, $R273_{Af}$ is positioned parallel to the ET-flavin, such that it stabilizes the negative charge delocalized over the flavin π system in the negatively charged states,[24,27,28,30,33,53] including via a π-cation interaction.[77] Positively charged $K523_{Sa}$ would preserve this interaction mediated by Arg in most bETFs. H-bond donation to N5 by S/T is understood to stabilize the ASQ state,[26] and $T540_{Sa}$'s position is consistent with retention of this interaction. Retention of the unusual H-bond from the ribose 4'OH to flavin N1 is also compatible with the model.[78] Preferential stabilization of the ASQ state of the ET-flavin has additionally been attributed to a H-bond donated to O2 from a His residue that is in turn supported by Tyr,[24,29] both of which are conserved in *Sa*ETF. In the *Sa*ETF model, $H560_{Sa}$ is well-positioned to donate a H-bond to the flavin O2, as in *Af*ETF,[33] and $Y549_{Sa}$ is positioned to donate a H-bond to the Nε of $H560_{Sa}$, thereby strengthening its H-bond donating capacity. These interactions are present in cETFs as well, so they do not specify bifurcating activity, but they all provide tuning important for the crucial and unusual 1e reactivity of the ET-FAD.

4.3. pH Dependence of E°s Is Consistent with ETF Reactivity

The 1e reactivity of ET-flavin rests on the stability of the SQ state relative to each of the OX and HQ states, embodied in the E°s. We measured E°s by both spcEC in solution and dirEC of *Sa*ETF immobilized on electrodes. The former allows for spectroscopic identification of the state of flavin formed but employs dyes/mediators that could interact with the system. Direct electrochemistry greatly facilitates variation of solution conditions and temperature but involves immobilizing the enzyme and any effects of the matrix used.[79] Considering these differences and accounting for the higher pH associated with the use of xanthine, along with the higher temperature needed to resolve events in dirEC, the agreement is remarkably good (Table 2).

Via our combination of methods, we used the pH dependence of the E° values to obtain a deeper understanding of the electrochemical behavior of *Sa*ETF and to expand our understanding of bifurcation. Both CV and SWV data show that Bf-FAD acquires $2H^+$ per 2e. One of these can most easily be explained by the uptake of a proton at N5, based on chemical precedent (Figure S1).[10] Acquisition of a second proton at the flavin's N1 position is associated with a pK_a of 6.7 in the HQ state for free flavin,[10] so it is a weak base that can plausibly be satisfied by hydrogen bonds in the binding site instead of a second proton.[24] Another nearby base could also be the acceptor in conjunction with the formation of AHQ for either flavin, because both binding sites contain a conserved Arg residue that could stabilize the AHQ. Unfortunately, it is not easy to distinguish the products predicted by these two possibilities based on optical spectra,[80] due to the overlapping spectra of the two flavins. We note that the $2H^+/2e$ stoichiometry may also not extend to the pH of 8.5 used for spcEC, because the calculation of the $^{Bf}E°_{OX/HQ}$ expected at pH 7, based on the $^{Bf}E°_{OX/HQ}$ at pH 8.5 and −60 mV/pH unit, overestimates the experimental value (−213 mV calculated vs −270 mV observed, Table 2). When the calculation employs −30 mV/pH, as expected for $1H^+/2e$, the result calculated for pH 7 is −257 mV, which is much closer to the observed value. Thus, it appears that a stoichiometry closer to $1H^+/2e$ applies at high pH, indicating that the HQ state of the Bf-FAD is associated with a pH near 8.5.

Direct EC was only able to resolve individual 1e E°s for the ET-FAD when elevated temperature was combined with low pH. Under these conditions, it was found that a proton is taken

https://doi.org/10.1021/jacsau.4c01219
JACS Au 2025, 5, 1689−1706

up for each of the two ET-FAD reductions between pH 6 and 7. However, spcEC documents the formation of ASQ at high pH and finds that $^{ET}E°_{OX/SQ}$ is not pH-dependent above pH 7.5. Thus, ^{ET}OX/SQ ceases to be coupled to proton uptake at pH > 7.5, indicating that the pK_a of the proton acceptor in the presence of ^{ET}SQ is near 7.5. This is slightly lower than pK_a normally associated with flavin's N5 of 8.5, but not unreasonable.[10] Thus, at low pH and 40 °C, *Sa*ETF may populate the NSQ.

Direct EC and spcEC agree regarding the acquisition of $1H^+/1e$ in the ^{ET}SQ/HQ couple over the entire pH range, as covered by spcEC at high pH and dirEC at 40 °C at lower pHs. At lower pHs, where the three redox events are all coupled to proton uptake, the pH contributes similarly to each of the E° values, so the separations between them should not be pH-dependent, preserving the sequence of oxidation states populated. However, at higher pH, when the initial reduction of ET-FAD is not coupled to flavin protonation, the resulting ASQ state is not subject to reduction unless a proton is available. In essence, the doubly anionic HQ state that would result from a second reduction is too unstable. Thus, at high pH, a dearth of protons can be considered to postpone the second reduction of ET-FAD, effectively stabilizing the ASQ. Table 2 provides maximal populations of ^{ET}SQ that would be stabilized at the midpoint between $^{ET}E°_{OX/SQ}$ and $^{ET}E°_{SQ/HQ}$, which are indicative of ET-FAD's tendency toward the 1e reactivity required for bifurcation, as opposed to the 2e reactivity more natural for free flavin. The aforementioned non-protonation of ET-FAD applicable at high pH in spcEC results in a robust population of ASQ. At pH 6 and 20 °C, dirEC demonstrates negligible SQ population, but increasing the temperature to 40 °C changes that, and the separation between observed ^{ET}E° values indicates that even at pH 6 (at 40 °C), more than half the sites can populate the ^{ET}SQ. Thus, although more studies are required to understand the effects of pH and temperature, both spcEC and dirEC document the ^{ET}SQ state, which is considered a crucial participant in bifurcating activity. The fact that ^{ET}ASQ is strongly populated in numerous ETFs over a range of pHs substantiates its significance[26,35,38,78] and suggests that the proton coupled to the ^{ET}OX/ASQ couple may be acquired by an amino acid side chain, not the flavin, satisfying both the pH dependence seen in dirEC and the spectra observed. Based on the identities of conserved amino acids near the ET-FAD, as well as the pK_a near 7.5 that applies to it, we propose that this residue is $His560_{Sa}$.

Besides the pH dependence of the E° values, the variation in pH had an important effect on what reactions could be observed. At pH > 7, neither CV nor SWV displayed a signature of the ET-FAD, and the use of elevated temperature was required to resolve signatures of the two individual 1e events seen in spcEC. Based on the pH dependence shown in Figure 7, a group with a pK_a in the range of 6−7 must be protonated to render any ET-FAD electrochemistry visible by dirEC at room temperature. At 40 °C, a pH of 7 or below is similarly required for ET-FAD's two sequential events to be perceived. ET-FAD remains present but appears disconnected from the electrode at high pH values and lower temperatures. We attribute this to a conformational change, as such changes have already been demonstrated for ETF,[12,62] and older work documents impaired electron transfer to/from the ET-FAD in at least one conformational state.[81] We note that spcEC enables detection of redox events much slower than those best studied by dirEC, and the dyes used in spcEC may retain access to the ET-FAD in the closed conformation. Thus, spcEC may be able to detect a redox event concealed from dirEC at high pH due to conformational change. Finally, the environment produced by the $MWCNT_{OH}$ may favor a different conformation than the one favored for *Sa*ETF diffusing in solution.

The best-documented conformational change in ETF is an 80° rotation of the head domain that carries the ET-FAD.[11,12,81] The two terminal orientations have been documented in crystal structures and produce quite different solvent-accessible surface areas for the ET-flavin in the known structures of *Af*ETF and *Aw*ETF.[11,33] Thus, a conformation that buries ET-flavin could suppress electron transfer between it and the electrode. In addition, work on *Af*ETF shows that binding to partner proteins significantly changes the E°s of the ET-flavin, altering the separation between them and thus the K_{SQ}.[32] Therefore, the ETF literature provides ample plausible explanations for the ET-FAD behavior we observe, wherein the population of ^{ET}SQ is sensitive to conformation and context. Our new finding in this regard is of a conformational event that is coupled to the protonation of a group with a pK_a in the range of 6 − 8 in *Sa*ETF and is more temperature-sensitive. This need not be identical to the conformational event associated with partner binding.

The pH range of 6−8, affecting electrochemical contact between ET-FAD and our electrodes, implicates a Cys or a His side chain. *Sa*ETF has only three Cys residues, and they are neither near the ET-flavin nor the interface between domains. However, the conserved His, $H560_{Sa}$ that we also propose as a redox-coupled proton acceptor, donates a hydrogen bond to the ET-flavin and tunes its E°.[24,29] Therefore, we speculate that the protonation state of this His could be coupled to the orientation of *Sa*ETF's head domain and the ET-FAD's accessibility to electrodes. His capacity to acquire a proton could, moreover, also be a source of the change in redox activity of ET-FAD observed upon complexation with its partner. Since this His is near the interface believed to contact partner proteins, its environment would be altered by binding, in turn changing His' pK_a. A drop in His' pK_a and loss of its proton would decrease stabilization of the ^{ET}ASQ, consistent with a switch to the 2e reactivity Sucharitakul et al. observe with the partner bound,[32] and we observe by dirEC at pH 6 and 20 °C. Our ability to observe both sequential 1e couples at 40 °C, vs a single 2e couple at 20 °C, provides us with a starting point for better understanding the ET-flavin's highly context-dependent electrochemical reactivity, which may serve to optimize the efficiency of electron transfer to its partner protein.

5. CONCLUSIONS AND FUTURE PROSPECTS

In archaea and bacteria, EtfB's gene is generally followed by that of EtfA (Figure 9). Accordingly, we demonstrate that a protein from *S. acidocaldarius* representing a concatenation of EtfB followed by EtfA has the properties and reactivity of a bifurcating ETF. Although our finding is not unexpected, the current work is the first biochemical characterization of a monomeric ETF. Structural and dynamic characterizations will be reported separately, as will phylogeny; however, NMR studies already document *Sa*ETF's excellent stability and solution behavior.[39] Thus, this novel architecture of ETF opens new possibilities for exploring relationships between subunit interactions, stability, conformational plasticity, tem-

https://doi.org/10.1021/jacsau.4c01219
JACS Au 2025, 5, 1689−1706

perature dependence, and the various parameters that can contribute to utility in bioelectrocatalytic deployment.[82,83]

*Sa*ETF's amenability to immobilization on electrodes paves the way for detailed studies of the mechanism of bifurcation via direct electrochemical means. Moreover, since *Sa*ETF displays a robust 2e cathodic wave for the Bf-flavin, an electrode can supply the two reducing equivalents needed for bifurcation, eliminating the expensive diffusible NADH substrate. If the resulting fully reduced Bf-flavin retains the ability to convey low-E° reducing equivalents to Fd or Fld upon 1e oxidation, we can hope to develop a bioelectrode able to provide low-E° electrons based on a modest voltage source, thereby lowering the barrier to capturing CO_2 or fixing N_2 by electrochemical means. Thus, the current work provides inspiration as to how biohybrid devices may be able to diminish barriers to demanding reactions required to safeguard the environment and meet human needs.

■ ASSOCIATED CONTENT

Supporting Information

The Supporting Information is available free of charge at https://pubs.acs.org/doi/10.1021/jacsau.4c01219.

> Twelve figures provide the structures of flavin in different reduction/protonation states (1 figure), more details regarding biochemical experiments (2 figures), direct electrochemistry comparisons and controls (7 figures), extended data supporting the sequence similarity networks and gene neighborhoods (2 figures), and some experimental details (PDF)

■ AUTHOR INFORMATION

Corresponding Authors

Shelley D. Minteer − *Kummer Institute Center for Resource Sustainability, Missouri University of Science and Technology, Rolla, Missouri 65409, United States;* orcid.org/0000-0002-5788-2249; Email: shelley.minteer@mst.edu

Anne-Frances Miller − *Department of Chemistry, University of Kentucky, Lexington, Kentucky 40506-0055, United States;* orcid.org/0000-0003-4973-2061; Email: afmill3r2@gmail.com

Authors

Debarati Das − *Department of Chemistry, University of Kentucky, Lexington, Kentucky 40506-0055, United States;* orcid.org/0000-0002-9956-1304

Wassim El Housseini − *Kummer Institute Center for Resource Sustainability, Missouri University of Science and Technology, Rolla, Missouri 65409, United States*

Monica Brachi − *Kummer Institute Center for Resource Sustainability, Missouri University of Science and Technology, Rolla, Missouri 65409, United States*

Complete contact information is available at: https://pubs.acs.org/10.1021/jacsau.4c01219

Author Contributions

Conceptualization: D.D. and A.F.M. Investigation and Methodology: D.D. and A.F.M. (samples and biochemistry) and W.E.H. and S.D.M. (electrochemistry). Resources: A.F.M. and S.D.M. Visualization: D.D., W.E.H., and A.F.M. Original draft: D.D., W.E.H., and A.F.M. Review and Editing: all. CRediT: **Debarati Das** conceptualization, investigation, methodology, visualization, writing - original draft, writing - review & editing; **Wassim El Housseini** investigation, methodology, visualization, writing - original draft, writing - review & editing; **Monica Brachi** writing - review & editing; **Shelley D. Minteer** funding acquisition, investigation, methodology, resources, supervision, writing - review & editing; **Anne-Frances Miller** conceptualization, funding acquisition, investigation, methodology, resources, supervision, visualization, writing - review & editing.

Funding

D.D. and A.F.M. gratefully acknowledge the support of the National Science Foundation Award CHE-2108134, and A.F.M. acknowledges partial support from DOE BES under DE- SC0021283. W.E.H., M.B., and S.D.M. were supported by the National Science Foundation Grant 2406605.

Notes

The authors declare no competing financial interest.

■ ACKNOWLEDGMENTS

We thank D.M. Bell for the expression vector (Leibniz-Forschungsinstitut für Molekulare Pharmakologie, Berlin-Buch, Germany), M.B. Das and Dr. D. Das for their encouragement, W.O.C. Miller for fearless grace, S.D. Miller, H. Oschkinat, and M.A Mroginski for their diligent oversight, and our anonymous reviewers for their valuable and constructive comments.

■ REFERENCES

(1) Nitschke, W.; Russell, M. J. Redox bifurcations: Mechanisms and importance to life now, and at its origin. *Bioessays* **2012**, *34*, 106−109.

(2) Herrmann, G.; Jayamani, E.; Mai, G.; Buckel, W. Energy conservation via electron-transferring flavoprotein in anaerobic bacteria. *J. Bacteriol.* **2008**, *190*, 784−791.

(3) Buckel, W.; Thauer, R. K. Energy conservation via electron bifurcating ferredoxin reduction and proton/Na+ translocating ferredoxin oxidation. *Biochim. Biophys. Acta, Protein Struct. Mol. Enzymol.* **2013**, *1827* (2), 94−113.

(4) Boucher, D. G.; Carroll, E.; Nguyen, Z. A.; Jadhav, R. G.; Simoska, O.; Beaver, K.; Minteer, S. D. Bioelectrocatalytic synthesis: Concepts and applications. *Angew. Chem., Int. Ed.* **2023**, *62*, No. e202307780.

(5) Chen, H.; Cai, R.; Patel, J.; Dong, F.; Chen, H.; Minteer, S. D. Upgraded bioelectrocatalytic N2 fixation: From N_2 to chiral amine intermediates. *J. Am. Chem. Soc.* **2019**, *141*, 4963−4971.

(6) Castañeda-Losada, L.; Adam, D.; Paczia, N.; Buesen, D.; Steffler, F.; Sieber, V.; Erb, T. J.; Richter, M.; Plumeré, N. Bioelectrocatalytic cofactor regeneration coupled to CO_2 fixation in a redox-active hydrogel for stereoselective C−C bond formation. *Angew. Chem., Int. Ed.* **2021**, *60*, 21056−21061.

(7) Chongpar, N.; Pawlak, K.; Rüdiger, O.; Reijerse, E. J.; Rodríguez-Marciá, P.; Lubitz, W.; Birrell, J. A.; Ogata, H. Spectroscopic and biochemical insight into an electron-bifurcating [FeFe] hydrogenase. *J. Biol. Inorg. Chem.* **2020**, *25*, 135−149.

(8) Lubner, C. E.; Jennings, D. P.; Mulder, D. W.; Schut, G. J.; Zadvornyy, O. A.; Hoben, J. P.; Tokmina-Lukaszewska, M.; Berry, L.; Nguyen, D. M.; Lipscomb, G. L. Mechanistic insights into energy conservation by flavin-based electron bifurcation. *Nat. Chem. Biol.* **2017**, *13* (6), 655−659.

(9) Wise, C. E.; Ledinina, A. E.; Mulder, D. W.; Chou, K. J.; Peters, J. W.; King, P. W.; Lubner, C. E. An uncharacteristically low-potential flavin governs the energy landscape of electron bifurcation. *Proc. Natl. Acad. Sci. U. S. A.* **2022**, *119* (12), No. e2117882119.

(10) Mayhew, S. G. The Effects of pH and Semiquinone Formation on the Oxidation-Reduction Potentials of Flavin Mononucleotide: A Reappraisal. *Eur. J. Biochem.* **1999**, *265*, 698−702.

(11) Demmer, J. K.; Bertsch, J.; Oppinger, C.; Wohlers, H.; Kayastha, K.; Demmer, U.; Ermler, U.; Muller, V. Molecular basis of the flavin-based electron-bifurcating caffeyl-CoA reductase reaction. *FEBS Lett.* **2018**, *592*, 332−342.
(12) Demmer, J. K.; Chowdhury, N. P.; Selmer, T.; Ermler, U.; Buckel, W. The semiquinone swing in the bifurcating electron transferring flavoprotein/butyryl-CoA dehydrogenase complex from Clostridium difficile. *Nat. Commun.* **2017**, *8* (1), 1577.
(13) Mazurenko, L.; Hitaishi, V. P.; Lojou, E. Recent advances in surface chemistry of electrodes to promote direct enzymatic bioelectrocatalysis. *Curr. Opin. Electrochem.* **2020**, *19*, 113−121.
(14) Savile, C. K.; Janey, J. M.; Mundorff, E. C.; Moore, J. C.; Tam, S.; Jarvis, W. R.; Colbeck, J. C.; Krebber, A.; Fleitz, F. J.; Brands, J. Biocatalytic Asymmetric Synthesis of Chiral Amines from Ketones Applied to Sitagliptin Manufacture. *Science* **2010**, *329* (5989), 305−309.
(15) Crane, K. L.; Beinert, H. On the mechanism of dehydrogenation of fatty acyl derivatives of coenzyme A. II. the electron transferring flavoprotein. *J. Biol. Chem.* **1956**, *218*, 717−731.
(16) Thorpe, C. Electron-Transferring Flavoproteins In *Chemistry and Biochemistry of Flavoenzymes*. 1st ed., Müller, F. Ed.; CRC press : 1991 pp. 471−486.
(17) Peters, J. W.; Miller, A. F.; Jones, A. K.; King, P. W.; Adams, M. W. Electron bifurcation. *Curr. Opin. Chem. Biol.* **2016**, *31*, 146−152.
(18) Buckel, W.; Thauer, R. K. Flavin-based electron bifurcation, a new mechanism of biological energy coupling. *Chem. Rev.* **2018**, *118* (7), 3862−3886.
(19) Müller, V.; Chowdhury, N. P.; Basen, M. Electron bifurcation: A long-hidden energy-coupling mechanism. *Annu. Rev. Microbiol.* **2018**, *72*, 331−353.
(20) Yuly, J. L.; Lubner, C. E.; Zhang, P.; Beratan, D. N.; Peters, J. W. Electron bifurcation: Progress and grand challenges. *Chem. Commun.* **2019**, *55*, 11823−11832.
(21) Hoben, J. P.; Lubner, C. E.; Ratzloff, M. W.; Schut, G. J.; Nguyen, D. M. N.; Hempel, K. W.; Adams, M. W. W.; King, P. W.; Miller, A.-F. Equilibrium and ultrafast kinetic studies manipulating electron transfer: A short-lived flavin semiquinone is not sufficient for electron bifurcation. *J. Biol. Chem.* **2017**, *292* (34), 14039−14049.
(22) Kayastha, K.; Katsyv, A.; Himmrich, C.; Welsch, S.; Schuller, J. M.; Ermler, U.; Müller, V. Structure-based electron-confurcation mechanism of the Ldh-EtfAB complex. *eLife* **2022**, *11*, No. e77095.
(23) Draper, R. D.; Ingraham, L. L. A potentiometric study of the flavin semiquinone equilibrium. *Arch. Biochem. Biophys.* **1968**, *125* (3), 802−808.
(24) González-Viegas, M.; Kar, R. K.; Miller, A. F.; Mroginski, M. A. Noncovalent interactions that tune the reactivities of the flavins in bifurcating electron transferring flavoprotein. *J. Biol. Chem.* **2023**, *299* (6), 104762.
(25) Ge, X.; Schut, G. J.; Tran, J.; Poole, F. L., II; Niks, D.; Menjivar, K.; Hille, R.; Adams, M. W. W. Characterization of the Membrane-Associated Electron-Bifurcating Flavoenzyme EtfABCX from the Hyperthermophilic Bacterium Thermotoga maritima. *Biochemistry* **2023**, *62* (24), 3554−3567.
(26) Yang, K. Y.; Swenson, R. P. Modulation of the redox properties of the flavin cofactor through hydrogen-bonding interactions with the N(5) atom: Role of αSer254 in the electron-transfer flavoprotein from the methylotrophic bacterium W3A1. *Biochem* **2007**, *46* (9), 2289−2297.
(27) Dwyer, T. M.; Zhang, L.; Muller, M.; Marrugo, F.; Frerman, F. E. The functions of the flavin contact residues αArg249 and βTyr16, in human electron transfer flavoprotein. *Biochim. Biophys. Acta, Protein Struct. Mol. Enzymol.* **1999**, *1433* (1−2), 139−152.
(28) Talfournier, F.; Munro, A. W.; Basran, J.; Sutcliffe, M. J.; Daff, S.; Chapman, S. K.; Scrutton, N. S. alpha Arg-237 in *Methylophilus methylotrophus* (sp. W3A1) electron-transferring flavoprotein affords approximately 200-millivolt stabilization of the FAD anionic semiquinone and a kinetic block on full reduction to the dihydroquinone. *J. Biol. Chem.* **2001**, *276* (23), 20190−20196.
(29) Das, D.; Miller, A.-F. A single hydrogen bond that tunes flavin redox reactivity and activates it for modification. *Chem. Sci.* **2024**, *15* (20), 7610−7622.
(30) Mohamed-Raseek, N.; Miller, A. F. Contrasting roles for two conserved arginines: Stabilizing flavin semiquinone or quaternary structure, in bifurcating electron transfer flavoproteins. *J. Biol. Chem.* **2022**, *298* (4), 101733.
(31) Duan, H. D.; Lubner, C. E.; Tokmina-Lukaszewska, M.; Gauss, G. H.; Bothner, B.; King, P. W.; Peters, J. W.; Miller, A. F. Distinct flavin properties underlie flavin-based electron bifurcation within a novel electron-transferring flavoprotein FixAB from *Rhodopseudomonas palustris*. *J. Biol. Chem.* **2018**, *293* (13), 4688−4701.
(32) Sucharitakul, J.; Buttranon, S.; Wongnate, T.; Chowdhury, N. P.; Prongjit, M.; Buckel, W.; Chaiyen, P. Modulations of the reduction potentials of flavin-based electron bifurcation complexes and semiquinone stabilities are key to control directional electron flow. *FEBS J.* **2021**, *288*, 1008−1026.
(33) Chowdhury, N. P.; Mowafy, A. M.; Demmer, J. K.; Upadhyay, V.; Koelzer, S.; Jayamani, E.; Kahnt, J.; Hornung, M.; Demmer, U.; Ermler, U. Studies on the mechanism of electron bifurcation catalyzed by electron transferring flavoprotein (Etf) and butyryl-CoA dehydrogenase (Bcd) of *Acidaminococcus fermentans*. *J. Biol. Chem.* **2014**, *289*, 5145−5157.
(34) Jumper, J.; Evans, R.; Pritzel, A.; Green, T.; Figurnov, M.; Ronneberger, O.; Tunyasuvunakool, K.; Bates, R.; Zidek, A.; Potapenko, A. Highly accurate protein structure prediction with AlphaFold. *Nature* **2021**, *596* (7873), 583−589.
(35) Mohamed-Raseek, N.; Diessel Duan, H.; Hildebrandt, P.; Mroginski, M. A.; Miller, A.-F. Spectroscopic, thermodynamic and computational evidence of the locations of the FADs in the nitrogen fixation-associated electron transfer flavoprotein. *Chem. Sci.* **2019**, *10*, 7762−7772.
(36) Vigil, W., Jr.; Tran, J.; Niks, D.; Schut, G. J.; Ge, X.; Adams, M. W. W.; Hille, R. The reductive half-reaction of two bifurcating electron-transferring flavoproteins: Evidence for changes in flavin reduction potentials mediated by specific conformational changes. *J. Biol. Chem.* **2022**, *298* (6), 101927.
(37) Sucharitakul, J.; Buckel, W.; Chaiyen, P. Rapid kinetics reveal surprising flavin chemistry in the bifurcating electron transfer flavoprotein from *Acidaminococcus fermentans*. *J. Biol. Chem.* **2021**, *296*, 100124.
(38) Sato, K.; Nishina, Y.; Shiga, K. Interaction between NADH and electron-transferring flavoprotein from *Megasphaera elsdenii*. *J. Biochem.* **2013**, *153* (6), 565−572.
(39) Bell, D.; Lindemann, F.; Gerland, L.; Aucharova, H.; Klein, A.; Friedrich, D.; Hiller, M.; Grohe, K.; van Rossum, B.; Diehl, A. Sedimentation of large, soluble proteins up to 140 kDa for 1H-detected MAS NMR and 13C DNP NMR − practical aspects. *J. Biomol. NMR* **2024**, *78* (3), 179−192.
(40) Sato, K.; Nishina, Y.; Shiga, K. Purification of electron-transferring flavoprotein from *Megasphaera elsdenii* and binding of additional FAD with an unusual absorption spectrum. *J. Biochem.* **2003**, *134* (5), 719−729.
(41) Haid, E.; Lehmann, P.; Ziegenhorn, J. Molar absorptivities of beta-NADH and beta-NAD at 260 nm. *Clin. Chem.* **1975**, *21* (7), 884−887.
(42) Mayhew, S. G. The redox potential of dithionite and SO^{-2} from equilibrium reactions with flavodoxins, methyl viologen and hydrogen plus hydrogenase. *Eur. J. Biochem.* **1978**, *85*, 535−547.
(43) Massey, V. A simple method for determination of redox potentials. In *Flavins and flavoproteins*, Curti, B.; Ronchi, S.; Zanetti, G. Eds.; Walter de Gruyer: 1991, pp. 59−66.
(44) Miller, A. F.; Duan, H. D.; Varner, T. A.; Mohamed-Raseek, N. Reduction midpoint potentials of bifurcating electron transfer flavoproteins. *Meth. Enzymol.* **2019**, *620*, 365−398.
(45) Wang, J.; Wang, W.; Kollman, P. A.; Case, D. A. Automatic atom type and bond type perception in molecular mechanical calculations. *J. Mol. Graphics Modell* **2006**, *25*, 247−260.

https://doi.org/10.1021/jacsau.4c01219
JACS Au 2025, 5, 1689−1706

(46) Wang, J.; Wolf, R. M.; Caldwell, J. W.; Kollman, P. A.; Case, D. A. Development and testing of a general AMBER force field. *J. Comput. Chem.* **2004**, *25*, 1157−1174.
(47) Pettersen, E. F.; Goddard, T. D.; Huang, C. C.; Couch, G. S.; Greenblatt, D. M.; Meng, E. C.; Ferrin, T. E. UCSF Chimera - a visualization system for exploratory research and analysis. *J. Comput. Chem.* **2004**, *25* (13), 1605−1612.
(48) Oberg, N.; Zallot, R.; Gerlt, J. A. EFI-EST, EFI-GNT, and EFI-CGFP: Enzyme Function Initiative (EFI) Web Resource for Genomic Enzymology Tools. *J. Mol. Biol.* **2023**, *435* (14), 168018.
(49) Zallot, R.; Oberg, N.; Gerlt, J. A. The EFI Web Resource for Genomic Enzymology Tools: Leveraging Protein, Genome, and Metagenome Databases to Discover Novel Enzymes and Metabolic Pathways. *Biochemistry* **2019**, *58* (41), 4169−4182.
(50) Müller, F.; Mayhew, S. G.; Massey, V. On the effeect of temperature on the absorption spectra of free and protein-bound flavines. *Biochem* **1973**, *12* (23), 4654−4662.
(51) Vigil, W., Jr.; Niks, D.; Franz-Badur, S.; Chowdhury, N.; Buckel, W.; Hille, R. Spectral deconvolution of redox species in the crotonyl-CoA-dependent NADH: Ferredoxin oxidoreductase from *Megasphaera elsdenii*. A flavin-dependent bifurcating enzyme. *Arch. Biochem. Biophys.* **2021**, *701*, 108793.
(52) Mohamed-Raseek, N.; van Galen, C.; Stanley, R.; Miller, A. F. Unusual reactivity of a flavin in a bifurcating electron-transferring flavoprotein leads to flavin modification and a charge-transfer complex. *J. Biol. Chem.* **2022**, *298* (12), 102606.
(53) Augustin, P.; Toplak, M.; Fuchs, K.; Gerstmann, E. C.; Prassl, R.; Winkler, A.; Macheroux, P. Oxidation of the FAD cofactor to the 8-formyl-derivative in human electron-transferring flavoprotein. *J. Biol. Chem.* **2018**, *293* (8), 2829−2840.
(54) Schut, G. J.; Mohamed-Raseek, N. R.; Tokmina-Lukaszewska, M.; Mulder, D. E.; Nguyen, D. M. N.; Lipscomb, G. L.; Hoben, J. P.; Patterson, A.; Lubner, C. E.; King, P. W. The catalytic mechanism of electron bifurcating electron transfer flavoproteins (ETFs) involves an intermediary complex with NAD+. *J. Biol. Chem.* **2019**, *294*, 3271−3283.
(55) Christgen, S. L.; Becker, S. M.; Becker, D. F. Methods for determining the reduction potentials of flavin enzymes. *Methods Enzymol.* **2019**, *620*, 1−25.
(56) Varničić, M.; Fellinger, T. P.; Titirici, M. M.; Sundmacher, K.; Vidaković-Koch, T. Rational Design of Enzymatic Electrodes: Impact of Carbon Nanomaterial Types on the Electrode Performance. *Molecules* **2024**, *29* (10), 2324.
(57) Cosnier, S.; Holzinger, M.; Le Goff, A. Recent Advances in Carbon Nanotube-Based Enzymatic Fuel Cells. *Front. Bioeng. Biotechnol.* **2014**, *2*, 00045.
(58) Zebda, A.; Gondran, C.; Le Goff, A.; Holzinger, M.; Cinquin, P.; Cosnier, S. Mediatorless high-power glucose biofuel cells based on compressed carbon nanotube-enzyme electrodes. *Nat. Commun.* **2011**, *2* (1), 370.
(59) Lopez-Tenes, M.; Gonzalez, J.; Molina, A. Two-electron transfer reactions in electrochemistry for solution-soluble and surface-confined molecules: A common approach. *J. Physs Chem. C* **2014**, *118* (23), 12312−12324.
(60) Siritanaratkul, B.; Megarity, C. F.; Herold, R. A.; Armstrong, F. A. Interactive biocatalysis achieved by driving enzyme cascades inside a porous conducting material. *Commun. Chem.* **2024**, *7* (1), 132.
(61) Dolińska, M. M.; Kirwan, A. J.; Megarity, C. F. Retuning the potential of the electrochemical leaf. *Faraday Discuss.* **2024**, *252*, 188−207.
(62) Demmer, J. K.; Huang, H.; Wang, S.; Demmer, U.; Thauer, R. K.; Ermler, U. Insights into flavin-based electron bifurcation via the NADH-dependent reduced ferredoxin: NADP oxidoreductase structure. *J. Biol. Chem.* **2015**, *290* (36), 21985−21995.
(63) Hirst, J. Elucidating the mechanisms of coupled electron transfer and catalytic reactions by protein film voltammetry. *Biochim. Biophys. Acta, Bioenerg.* **2006**, *1757* (4), 225−239.
(64) Chowdhury, N. P.; Kahnt, J.; Buckel, W. Reduction of ferredoxin or oxygen by flavin-based electron bifurcation in *Megasphaera elsdenii*. *FEBS J.* **2015**, *282*, 3149−3160.
(65) Ledbetter, R. N.; Garcia Costas, A. M.; Lubner, C. E.; Mulder, D. E.; Tokmina-Lukaszewska, M.; Artz, J. H.; Patterson, A.; Magnuson, T. S.; Jay, Z. J.; Duan, H. D. The electron bifurcating FixABCX protein complex from *Azotobacter vinelandii*: Generation of low-potential reducing equivalents for nitrogenase catalysis. *Biochemistry* **2017**, *56* (32), 4177−4190.
(66) Fischbach, M.; Voigt, C. A. Prokaryotic gene clusters: A rich toolbox for synthetic biology. *Biotechnol. J.* **2010**, *5* (12), 1277−1296.
(67) Mihelčić, M.; Šmuc, T.; Supek, F. Patterns of diverse gene functions in genomic neighborhoods predict gene function and phenotype. *Sci. Rep.* **2019**, *9* (1), 19537.
(68) Earl, C. D.; Ronson, C. W.; Ausubel, F. M. Genetic and structural analysis of the Rhizobium meliloti fixA, fixB, fixC, and fixX genes. *J. Bacteriol.* **1987**, *169* (3), 1127−1136.
(69) Garcia Costas, A. M.; Poudel, S.; Miller, A.-F.; Schut, G. J.; Ledbetter, R. N.; Fixen, K.; Seefeldt, L. C.; Adams, M. W.; Harwood, C. S.; Boyd, E. S.; et al. Defining electron bifurcation in the electron transferring flavoprotein family. *J. Bacteriol.* **2017**, *199*, 10−1128.
(70) Zuchan, K.; Baymann, F.; Baffert, C.; Brugna, M.; Nitschke, W. The dyad of the Y-junction- and a flavin module unites diverse redox enzymes. *Biochim. Biophys. Acta, Bioenerg.* **2021**, *1862* (6), 148401.
(71) Caetano-Anollés, G.; Wang, M.; Caetano-Anollés, D.; Mittenthal, J. E. The origin, evolution and structure of the protein world. *Biochem. J.* **2009**, *417* (3), 621−637.
(72) Doolittle, R. F. The multiplicity of domains in proteins. *Annu. Rev. Biochem.* **1995**, *64*, 287−314.
(73) Tordai, H.; Nagy, A.; Farkas, K.; Bányai, L.; Patthy, L. Modules, multidomain proteins and organismic complexity. *FEBS J.* **2005**, *272* (19), 5064−5078.
(74) Bystrom, L. T.; Wolthers, K. R. New Electron-Transfer Chain to a Flavodiiron Protein in *Fusobacterium nucleatum* Couples Butyryl-CoA Oxidation to O2 Reduction. *Biochem* **2024**, *63*, 2352−2368.
(75) Kabir, M. P.; Orozco-Gonzalez, Y.; Gozem, S. Electronic Spectra of Flavin in Different Redox and Protonation States: A Computational Perspective on the Effect of the Electrostatic Environment. *Chem. Chem. Phy.s* **2019**, *21*, 16526−16537.
(76) Kar, R. K.; Miller, A.-F.; Mroginski, M. A. Understanding flavin electronic structure and spectra. *Wiley Interdiscip. Rev.: Comput. Mol. Sci.* **2022**, *12*, No. e1541.
(77) Dougherty, D. A. The Cation−π Interaction. *Acc. Chem. Res.* **2013**, *46*, 885−893.
(78) Dwyer, T. M.; Mortl, S.; Kemter, K.; Bacher, A.; Fauq, A.; Frerman, F. E. The intraflavin hydrogen bond in human electron transfer flavoprotein modulates redox potentials and may participate in electron transfer. *Biochem* **1999**, *38*, 9735−9745.
(79) Sheldon, R. A.; van Pelt, S. Enzyme immobilisation in biocatalysis: Why, what and how. *Chem. Soc. Rev.* **2013**, *42* (15), 6223−6235.
(80) Yalloway, G. N.; Mayhew, S. G.; Malthouse, J. P. G.; Gallagher, M. E.; Curley, G. P. pH-dependent spectroscopic changes associated with the hydroquinone of FMN in Flavodoxins. *Biochem* **1999**, *38*, 3753−3762.
(81) Toogood, H. S.; Leys, D.; Scrutton, N. S. Dynamics driving function: New insights from electron transferring flavoproteins and partner complexes. *FEBS J.* **2007**, *274*, 5481−5504.
(82) Oh, J.; Durai, P.; Kannan, P.; Park, J. T.; Yeon, Y. J.; Lee, W.-K.; Park, K.; Seo, M.-H. Domain-wise dissection of thermal stability enhancement in multidomain proteins. *Int. J. Biol. Macromol.* **2023**, *237*, 124141.
(83) Chakravorty, D.; Khan, M. F.; Patra, S. Multifactorial level of extremostability of proteins: Can they be exploited for protein engineering? *Extremophiles* **2017**, *21*, 419−444.

https://doi.org/10.1021/jacsau.4c01219
JACS Au 2025, 5, 1689−1706